A Displacement Based FE Formulation for Steady State Problems

This research was carried out under project number $ME97034$ in the framework of the Strategic Research programme of the Netherlands Institute of Metals Research in the Netherlands (www.nimr.nl)

Samenstelling van de promotiecommissie:

voorzitter en secretaris:	
Prof. dr. ir. H.J. Grootenboer	Universiteit Twente
promotor:	
Prof. dr. ir. J. Huétink	Universiteit Twente
leden:	
Prof. dr. ir. R. Akkerman	Universiteit Twente
Dr. ir. H.J.M. Geijselaers	Universiteit Twente
Prof.dr.ir. F.J.A.M. van Houten	Universiteit Twente
Prof. ir. L.Katgerman	Technische Universiteit Delft
Prof.dr.ir. H.J.J. Slot	DSM en Universiteit Twente

A Displacement Based FE Formulation for Steady State Problems

Yuhong Yu

Met samenvatting in het Nederlands

ISBN 90-77172-13-0

Keywords: elastic-plasticity, steady state flow processes, material evolution equation, finite element

This thesis was prepared with LaTeX by the author and printed by Ponsen & Looijen, Wageningen, from an electronic document.

A DISPLACEMENT BASED FE FORMULATION FOR STEADY STATE PROBLEMS

PROEFSCHRIFT

ter verkrijging van
de graad van doctor aan de Universiteit Twente,
op gezag van de rector magnificus,
prof. dr. W.H.M. Zijm,
volgens besluit van het College voor Promoties
in het openbaar te verdedigen
op woensdag 12 januari 2005 om 13.15 uur

door

Yuhong Yu

geboren op 9 augustus 1970
te Wuhan, China

Dit proefschrift is goedgekeurd door de promotor:

Prof. dr. ir. J. Huétink

Contents

Summary

The efficiency and accuracy of many traditional industrial forming processes may still be improved by application of numerical simulations. Many forming processes such as rolling, extrusion, continuous casting etc., behave as a steady state process. In recent years special methods have been developed for numerical simulation of steady processes and new contributions are still being published.

In this thesis a new displacement based formulation is developed for elasto-plastic deformations in steady state problems. In this formulation the displacements are the primary variables, which is in contrast to the more common formulations in terms of the velocities as the primary variables. In a steady state process, a transient calculation is not required and only space discretizations are needed, without time discretizations. The evolution of the material variables is expressed as an integration along the streamlines. The resulting differential equation describes steady convection with source terms.

The thesis is outlined as follows. The second chapter involves the theory of continuum mechanics. Hypo-elasticity and hyper-elasticity are introduced. In Chapter 3 a review of recent literature on the simulation of the steady state forming processes is presented. The method published by Balagangadhar appears to be most interesting. The development of our method is based on this work.

In chapter 5 our new method for simulation of steady elasto-plastic processes is presented. Several bottlenecks in Balagangadhar's work have been identified and solutions to them are presented. The formulation is very much simplified. The convection equation that describes the integration along the streamlines is transformed to the undeformed configuration. To calculate the material evolution by the convection equation, the Least Squares method appears to be the most suitable method. In this way the numerical oscillations, which are common in other formulations, are avoided almost totally. The calculation of the material derivatives of the state variables is improved by using an approximation by means of a continuous field. Also an algorithm is developed for modelling of the contact problem between tools and work

piece, which is consistent with the steady state solution method.

In Chapter 6 the developed method is applied successfully to a pure shear test and a simple two-dimensional extrusion problem.

Even though our numerical experiments are limited to a simple geometry and a rigid tool contact, the applicability of our method is demonstrated. It provides the possibility to improve the steady state flow simulation and points out a new direction in the field of the modelling of the steady state processes.

Samenvatting

Bij veel traditionele omvormprocessen kunnen numerieke simulaties bijdragen aan de verbetering van het procesverloop. Nauwkeurigheid en doelmatigheid kunnen op deze wijze worden verhoogd en de kosten verlaagd. Bij een aantal processen, zoals walsen, extrusie en continu gieten, is sprake van een stationair proces. In de afgelopen jaren is de ontwikkeling van algoritmen voor simulatie van stationaire processen onderwerp van onderzoek geweest binnen een selecte kring van onderzoekers. Ook nu nog worden regelmatig bijdragen op dit gebied gepubliceerd.

In dit proefschrift wordt een nieuwe formulering voor stationaire elasto-plastische omvormprocessen uitgewerkt. In deze formulering zijn de verplaatsingen de primaire variabelen. Dit is in tegenstelling tot de meer gebruikelijke formulering in termen van snelheden. Omdat er sprake is van een stationair proces, is een transiënte berekening niet nodig, de tijdsintegratie is vervangen door integratie langs de stroomlijnen. De evolutie van de toestandsvariabelen langs de stroomlijnen wordt uitgedrukt in een differentiaalvergelijking, die stationaire convectie beschrijft.

In het proefschrift, dat voor U ligt, komen de volgende onderwerpen aan bod. In het tweede hoofdstuk worden de basis vergelijkingen uit de continuum mechanica behandeld. Vergelijkingen voor zowel een hypo-elastisch als een hyper-elastisch materiaalmodel worden afgeleid. Hoofdstuk 3 behelst een literatuur onderzoek naar simulatie van stationaire elasto-plastische omvormprocessen. De methode van Balagangadhar komt hierbij als meest belovend te voorschijn. De ontwikkeling van onze methode is gebaseerd op zijn werk.

Onze nieuwe methode voor simulatie van de stationaire elasto-plastic processen wordt gepresenteerd in hoofdstuk 5. Een aantal knelpunten in de methode van Balagangadhar zijn geïdentificeerd en oplossingen hiervoor worden aangedragen. De formulering is sterk vereenvoudigd. De convectievergelijking, die de stroomlijn integratie beschrijft, wordt getransformeerd naar de onvervormde configuratie. Voor het oplossen van de convectievergelijking blijkt de kleinste kwadraten methode het meest geschikt. De numerieke instabiliteiten, die bij veel oplossingsmethoden voor convectiev-

ergelijkingen optreden zijn vrijwel afwezig. De berekening van de materiële afgeleiden van de toestandsvariabelen is verbeterd door gebruik te maken van een benadering door middel van continue velden. Ook is voor modellering van het contact tussen gereedschap en werkstuk een contact-algoritme ontwikkeld, dat past bij een stationaire oplosmethode.

In hoofdstuk 6 is de ontwikkelde methode met succes toegepast op een modelprobleem met zuivere afschuiving en op een eenvoudig twee-dimensionaal extrusieprobleem.

Hoewel onze numerieke experimenten tot een eenvoudige geometrie en een stijf gereedschapscontact beperkt zijn, wordt de bruikbaarheid van onze methode aangetoond. Het verstrekt de mogelijkheid om de simulatie van de stationaire vormgevings processen te verbeteren en wijst een nieuwe richting op het gebied van de modellering van dit soort processen.

Chapter 1

Introduction

Why do research? History provides the answer

1.1 Industrial Revolution and Development

Beyond all doubt technology increasingly plays a strategic role in the development of the economy all over the world. Industry is the key generator of resources for further economic development. Therefore, without the application of inventions and new technologies in industrial life, social and economic evolution would and will terminate.

Two well-known industrial revolutions started with the utilization of new

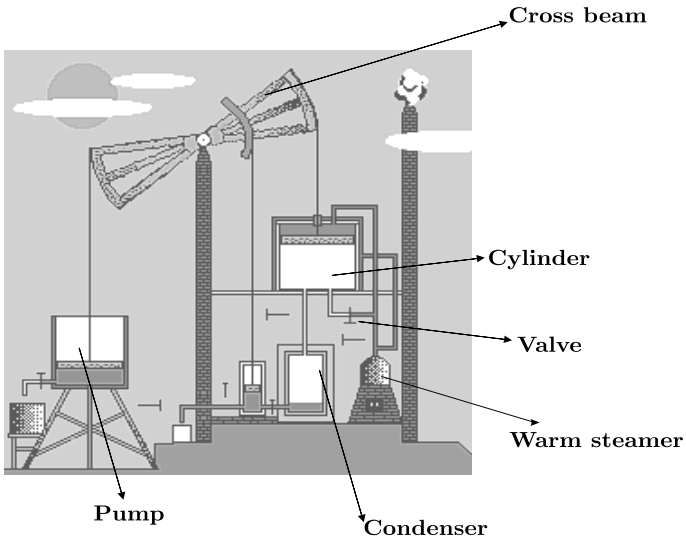

Figure 1.1: A model of the Watt engine for pumping

technologies ([2],[3]). The First Industrial Revolution took place in Great Britain around 1750. This First Industrial Revolution resulted from the invention of three types of the machine: the steam engine (see Fig. 1.1), machines for spinning thread and weaving cloth and furnaces (e.g. to make ironstone into finished metal). These machines made mass production possible and put the cottage industry into historic memory.

After the harsh depression of the 1870*s*, the Second Industrial Revolution results from innovations in the production of materials (metals etc.), chemicals and foodstuffs and the centre of the revolution moved from the UK to the US and Germany. Three stages were achieved during this revolution. First, the transportation and communication networks (telegraph, railroad and cable) were built up; second, the development of electricity offered a new source of power for industry field; third, science began to be applied to industrial processes to create the products as demanded. In brief, the industrial revolutions shaped the modern society into what it is today.

Since the second industrial revolution, with the extensive development of science and technology, the computer-driven information revolution is exerting a strong influence on all corners of the world. In industry, computers are playing an important role in industrial design, quality control, business operation and process modelling. The modelling of metal forming processes aims to reach a better understanding and optimization of the processes by use of numerical techniques. A process model requires the combination of different fields of knowledge, such as mathematics, mechanics, material science and also computational skills.

1.2 Project Definition

As is well known, many manufacturing processes such as rolling, extrusion, continuous casting, laser welding etc., behave as steady state processes. Finite element analysis of these steady state processes has mainly been done with Lagrangian, Eulerian and Arbitrary Lagrangian-Eulerian(ALE) descriptions. However, these models have some disadvantages for steady state problems.

In the Lagrangian formulation the evolutionary nature of the plasticity can be followed by an incremental analysis. The simulation terminates when the steady state is reached. But it is time-consuming and the interaction between the time and space discretizations could lead to numerical oscillations. In a Eulerian formulation the material flows through a fixed domain in space. The problems are calculated on the whole concerned domain at once, instead of using incremental steps as in a Lagrangian formulation. In order to obtain the material state variables (e.g. the stress or the cumulative plastic strain), integration of the evolution equations must be carried out along

the streamlines. These streamlines are not known a priori in the deformed configuration. Therefore, iterative techniques are required. When a segment of the boundary is a free surface, iterative steps are needed to adjust these parts of the boundary in order for it to coincide with the streamlines. A combined Lagrangian and Eulerian formulation called the Arbitary Lagrangian-Eulerian (ALE) method has been developed to solve the problems which occur in the two traditional methods described above. As in the Eulerian formulation, in order to handle history dependent material variables, convection must be taken into account. As in the Lagrangian formulation, ALE is still calculated transiently. In conclusion, all three methods cause problems to some extent during the simulation.

The present research project was proposed as result of a thorough literature review for steady state process simulation. The challenge was to develop a displacement based steady state formulation. Indeed, the idea of the project was suggested by the work of Balagangadhar ([1]). The objective of this project will be discussed in more detail in Chapter 3.

1.3 Overview of the Thesis

The thesis includes another six further chapters:

Chapter 2 concerns continuum mechanics. It provides the theoretical background for our work. In this chapter the material models are described that were used for the simulation. For our case, the available material models were chosen for different situations during processing. For the small deformation case, the linear elastic-plastic model can be applied, but for the large deformation case, the hyperelastic-plastic model was chosen. The question of when to use hyperelasticity instead of hypoelasticity the answer is investigated in this chapter.

Chapter 3 contains a literature review of the previous work on models for the simulation of steady state manufacturing processes. Balagangadhar's work is the central theme of this chapter.

Chapter 4 discusses the finite element method. In this chapter the linearized theory and finite element discretizations are included.

Chapter 5 includes the displacement based formulation posed on the steady state nature. The stabilized FEM and the contact analysis for this case are included in this chapter.

Chapter 6 includes the results for the different situations. The results are also discussed here.

Chapter 7 concludes the thesis with the conclusions and recommendations for future improvements.

At the end of every chapter a bibliography is listed.

Bibliography

[1] Balagangadhar, D., Tortorelli, D.A.: Design of steady state processes via a displacement based reference frame formulation. In Simulation of Materials Processing: Theory, Methods and Applications, Huetink and Baaijens (Eds), NUMIFORM'98, Enschede, Balkema, 1998, 77-83

[2] Chandler, Jr.Alfred D.: The Visible Hand, The Managerial Revolution in American Business, 1977

[3] Mathias, P.: The First Industrial Nation: An Economic History of Britain, 2nd ed., 1983

[4] Kitano, K., Morejon, A.: Essay on the industrial revolution: A trip to past, http://members.aol.com/mhirotsu/essay.htm

Chapter 2

Continuum Mechanics

Basis for finite element analysis

This chapter is a summary of continuum mechanics and it provides the theoretical support for the finite element (FE) method, which was used for the modelling work. In the first part of this chapter, some concepts of deformation are presented. Further on, the definitions of stress and strain are described. The conservation equations, also called the balance equations, are introduced and hence the equilibrium equations that are described in the different configurations.

2.1 Basic Concepts of Deformation

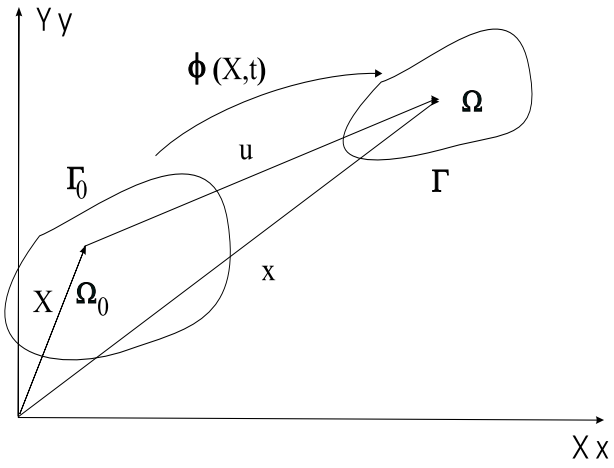

Figure 2.1: Initial and current configurations of a body

At time t_0 we consider a body (see Fig. 2.1) within a domain Ω_0 bounded by Γ_0, which we call the initial configuration. We call the initial configuration the *undeformed configuration*. In order to describe the motion and deformation of the body, a referential configuration is needed to define the motion. The initial configuration is mostly used as the referential configuration. After a certain time, the body is moved or deformed to the domain Ω with boundary Γ. This current configuration is called the *deformed configuration*.

The position field of a material point in the referential configuration is expressed by $\mathbf{X}$, which is called the material or Lagrangian coordinate. Meanwhile, the position vector of a point in the current or deformed configuration is given by $\mathbf{x}$, which is the spatial or Eulerian coordinate. The relation between these two positions is described by the motion of the body:

$$\mathbf{x} = \boldsymbol{\phi}(\mathbf{X}, t) \tag{2.1}$$

where $\boldsymbol{\phi}$ is the mapping function from the referential configuration to the current configuration at time t. The position $\mathbf{x}$ at time $t = 0$ coincides with the material coordinates, when the referential configuration coincides with the initial configuration. There are two descriptions for the deformation and motion of a continuum. One is called a material or Lagrangian description, in which the independent variables are the material coordinates. The other is called a spatial or Eulerian description in which the independent variables are the spatial coordinates. When the same field is expressed in terms of different descriptions, such as the Eulerian or Lagrangian descriptions, the different function symbols are used as follows:

$$(\mathbf{X}, t) = f(\boldsymbol{\phi}(\mathbf{X}, t), t) \tag{2.2}$$

The displacement $\mathbf{u}$ of a material point can be obtained from the difference between its original and current positions:

$$\mathbf{u}(\mathbf{X}, t) = \boldsymbol{\phi}(\mathbf{X}, t) - \boldsymbol{\phi}(\mathbf{X}, 0) = \mathbf{x} - \mathbf{X} \tag{2.3}$$

An important notion is the deformation gradient, which is defined as:

$$\mathbf{F} = \frac{\partial \boldsymbol{\phi}}{\partial \mathbf{X}} = \frac{\partial \mathbf{x}}{\partial \mathbf{X}} = \mathbf{I} + \frac{\partial \mathbf{u}}{\partial \mathbf{X}} \tag{2.4}$$

The determinant J of $\mathbf{F}$ is the relative volume. $\mathbf{I}$ is the unit tensor.

2.2 Strain and Stress

The concepts of strain and stress are introduced to define the deformation and motion of the continuum body. In this section the strain and stress measures are described respectively. Later the frame invariance and objectivity will be defined.

2.2.1 Strain Measure

The Green (Green-Lagrange) strain $\mathbf{E}$ is defined to measure the change in the squared length of an infinitesimal segment with reference to the material elemental vector $d\mathbf{X}$, while the body deforms from the referential (undeformed) configuration to the current configuration:

$$ds^2 - dS^2 = d\mathbf{x} \cdot d\mathbf{x} - d\mathbf{X} \cdot d\mathbf{X} = 2d\mathbf{X} \cdot \mathbf{E} \cdot d\mathbf{X} \tag{2.5}$$

Using Eq. (2.4), we have:

$$d\mathbf{x} = \mathbf{F} \cdot d\mathbf{X} \tag{2.6}$$

Thus:

$$d\mathbf{x} \cdot d\mathbf{x} = (\mathbf{F}\, d\mathbf{X})^T \cdot (\mathbf{F}\, d\mathbf{X}) = d\mathbf{X} \cdot (\mathbf{F}^T \cdot \mathbf{F}) \cdot d\mathbf{X} \tag{2.7}$$

Substitute Eq. (2.7) into Eq. (2.5):

$$d\mathbf{X} \cdot (\mathbf{F}^T \cdot \mathbf{F} - \mathbf{I}) \cdot d\mathbf{X} = 2d\mathbf{X} \cdot \mathbf{E} \cdot d\mathbf{X} \tag{2.8}$$

Therefore:

$$\mathbf{E} = \frac{1}{2}(\mathbf{F}^T \cdot \mathbf{F} - \mathbf{I}) \tag{2.9}$$

where the right Cauchy-Green deformation tensor is defined as:

$$\mathbf{C} = \mathbf{F}^T \cdot \mathbf{F} \tag{2.10}$$

Then the Green Lagrange strain tensor is defined as:

$$\mathbf{E} = \frac{1}{2}(\mathbf{C} - \mathbf{I}) \tag{2.11}$$

This strain tensor is expressed in terms of the displacement gradient by:

$$\mathbf{E} = \frac{1}{2}((\nabla_0 \mathbf{u})^T + \nabla_0 \mathbf{u} + \nabla_0 \mathbf{u} \cdot (\nabla_0 \mathbf{u})^T) \tag{2.12}$$

with:

$$\nabla_0 \mathbf{u} = (\frac{\partial \mathbf{u}}{\partial \mathbf{X}})^T \tag{2.13}$$

Alternatively, the same length change can be derived with reference to the spatial elemental vector $d\mathbf{x}$ as:

$$ds^2 - dS^2 = 2d\mathbf{x} \cdot \mathbf{e} \cdot d\mathbf{x} \tag{2.14}$$

where $\mathbf{e}$ is called the Eulerian or Almansi strain tensor. This strain tensor can be expressed in terms of the displacement gradient by:

$$\mathbf{e} = \frac{1}{2}((\nabla \mathbf{u})^T + \nabla \mathbf{u} - \nabla \mathbf{u} \cdot (\nabla \mathbf{u})^T) \tag{2.15}$$

with:

$$\nabla \mathbf{u} = (\frac{\partial \mathbf{u}}{\partial \mathbf{x}})^T \tag{2.16}$$

For the small deformation case, when the initial and final positions of a material point are practically the same, the quadratic term can be ignored. These two strain definitions become identical for small deformation.

2.2.2 Stress Measure

In classical continuum mechanics, four stress descriptions are used:

- The Cauchy stress tensor $\boldsymbol{\sigma}$;
- The nominal stress $\mathbf{P}$, $\mathbf{P}^T$is called the first Piola-Kirchhoff stress tensor;
- The Kirchhoff stress tensor $\boldsymbol{\tau}$;
- The second Piola-Kirchhoff stress tensor $\mathbf{S}$.

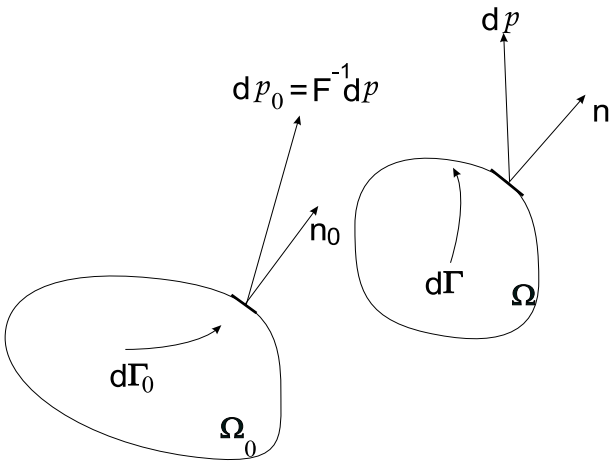

Figure 2.2: Force vectors for stress definitions

The Cauchy stress is defined in the current configuration using the equilibrium of the deformable body. The result is that the traction vector $\mathbf{t}$ at a point on the surface $\mathbf{d\Gamma}$ with outward normal $\mathbf{n}$ can be expressed in terms of the Cauchy stress tensor as:

$$d\boldsymbol{p} = \mathbf{t}\, d\Gamma = \mathbf{n} \cdot \boldsymbol{\sigma}\, d\Gamma \tag{2.17}$$

where $d\boldsymbol{p}$ is the force acting on a deformed element with area $d\Gamma$ and $\mathbf{t} = \mathbf{n}\cdot\boldsymbol{\sigma}$. The nominal tensor $\mathbf{P}$ can be derived as follows, see Fig. 2.2. We have ([1],[3],[4]):

$$\mathbf{n}\, d\Gamma = J\mathbf{n}_0 \cdot \mathbf{F}^{-1}\, d\Gamma_0 \tag{2.18}$$

We equal $d\boldsymbol{p}$ written in terms of the Cauchy stress and the nominal stress:

$$d\boldsymbol{p} = J\mathbf{n}_0 \cdot \mathbf{F}^{-1} \cdot \boldsymbol{\sigma}\, d\Gamma_0 = \mathbf{n}_0 \cdot \mathbf{P}^T d\Gamma_0 \tag{2.19}$$

The nominal stress tensor $\mathbf{P}$ has the form:

$$\mathbf{P} = J\boldsymbol{\sigma} \cdot \mathbf{F}^{-T} \tag{2.20}$$

where $\mathbf{P}$ is a non-symmetric tensor and expresses the force in the current configuration in terms of the area in the initial configuration.
The Kirchhoff stress tensor $\boldsymbol{\tau}$ is defined as:

$$\boldsymbol{\tau} = J\boldsymbol{\sigma} = \mathbf{P} \cdot \mathbf{F}^T \tag{2.21}$$

The second Piola-Kirchhoff stress $\mathbf{S}$ is obtained by pulling back the spatial force $d\boldsymbol{p}$ to a material force vector $d\boldsymbol{p}_0$:

$$d\boldsymbol{p}_0 = \mathbf{F}^{-1} \cdot d\boldsymbol{p} = \mathbf{n}_0 \cdot \mathbf{S} d\Gamma_0 \tag{2.22}$$

Using Eq. (2.19) we have:

$$\mathbf{S} = J\mathbf{F}^{-1} \cdot \boldsymbol{\sigma}\mathbf{F}^{-T} \tag{2.23}$$

Therefore $\mathbf{S}$ is symmetric.

2.2.3 Objectivity or Frame Indifference

Objectivity or frame indifference is an important concept in solid mechanics. The material constitutive relation should be independent of any rigid body motions. Many quantities describing the material behaviour should be observed as being the same by two different observers in relative rotation and translation. This is called the principle of material objectivity or material frame indifference.

Let $\tilde{\mathbf{x}}$ result from $\mathbf{x}$ by rotation ($\mathbf{Q}$) and translation ($\boldsymbol{l}$) of the reference frame:

$$\tilde{\mathbf{x}} = \mathbf{Q} \cdot \mathbf{x} + \boldsymbol{l} \qquad \text{and } \mathbf{Q}^{-1} = \mathbf{Q}^T \tag{2.24}$$

It follows that:

$$d\tilde{\mathbf{x}} = \mathbf{Q} \cdot d\mathbf{x} = \mathbf{Q} \cdot \mathbf{F} \cdot d\mathbf{X} \tag{2.25}$$

Although this vector $d\tilde{\mathbf{x}}$ differs from $d\mathbf{x}$, their magnitudes are equal. In this case the $d\mathbf{x}$ is objective under rigid motion.

For Eulerian, Lagrangian and Eulerian-Lagrangian tensors, in general there are different definitions to judge whether these tensors are objective or not ([1]). A Eulerian vector $\mathbf{a}$ and a Eulerian second order tensor $\mathbf{A}$ are said to be objective if:

$$\tilde{\mathbf{a}} = \mathbf{Q} \cdot \mathbf{a}, \quad \tilde{\mathbf{A}} = \mathbf{Q} \cdot \mathbf{A} \cdot \mathbf{Q}^T \tag{2.26}$$

A Lagrangian vector $\mathbf{a}$ and a Lagrangian second order tensor $\mathbf{A}$ are said to be invariant if:

$$\tilde{\mathbf{a}}_0 = \mathbf{a}_0, \quad \tilde{\mathbf{A}}_0 = \mathbf{A}_0 \tag{2.27}$$

A Eulerian-Lagrangian second order tensor $\mathbf{A}$ is said to be objective if:

$$\tilde{\mathbf{A}} = \mathbf{Q} \cdot \mathbf{A} \tag{2.28}$$

For example, the deformation tensor $\mathbf{F}$ is called an objective Eulerian-Lagrangian second order tensor since:

$$\tilde{\mathbf{F}} = \mathbf{Q} \cdot \mathbf{F} \tag{2.29}$$

The time derivative of the second Piola-Kirchhoff stress tensor $\mathbf{S}$ is invariant. But the time derivative of the Cauchy stress tensor $\boldsymbol{\sigma}$ is clearly non-objective:

$$\dot{\tilde{\boldsymbol{\sigma}}} = \dot{\mathbf{Q}} \cdot \boldsymbol{\sigma} \cdot \mathbf{Q}^T + \mathbf{Q} \cdot \dot{\boldsymbol{\sigma}} \cdot \mathbf{Q}^T + \mathbf{Q} \cdot \boldsymbol{\sigma} \cdot \dot{\mathbf{Q}}^T \tag{2.30}$$

In the rate-type constitutive equations the objective rates should be constructed by the so-called pull-back push-forward procedure. The *Truesdell stress rate* $\tilde{\boldsymbol{\sigma}}^{\triangledown}$ is thus defined in terms of the transformation of the time derivative of the second Piola-Kirchhoff stress as ([3],[4]):

$$\tilde{\boldsymbol{\sigma}}^{\triangledown} = J^{-1} \cdot \mathbf{F}[\frac{d}{dt}(J \cdot \mathbf{F}^{-1} \cdot \boldsymbol{\sigma} \cdot \mathbf{F}^{-T})] \cdot \mathbf{F}^T \tag{2.31}$$

This can be worked out as:

$$\tilde{\boldsymbol{\sigma}}^{\triangledown} = \dot{\boldsymbol{\sigma}} - \mathbf{L} \cdot \boldsymbol{\sigma} - \boldsymbol{\sigma} \cdot \mathbf{L}^T + tr(\mathbf{L})\boldsymbol{\sigma} \tag{2.32}$$

The *Green-Naghdi stress rate* $\tilde{\boldsymbol{\sigma}}^{\triangle}$ is defined when the pull back and push forward operation is performed using only the rotation tensor $\mathbf{R}$:

$$\tilde{\boldsymbol{\sigma}}^{\triangle} = \mathbf{R} \cdot [\frac{d}{dt}(\mathbf{R}^T \cdot \boldsymbol{\sigma} \cdot \mathbf{R})] \cdot \mathbf{R}^T = \dot{\boldsymbol{\sigma}} - \boldsymbol{\sigma} \cdot \dot{\mathbf{R}} \cdot \mathbf{R}^T - \dot{\mathbf{R}} \cdot \mathbf{R}^T \boldsymbol{\sigma} \tag{2.33}$$

If the antisymmetric tensor $\dot{\mathbf{R}} \cdot \mathbf{R}^T$ is approximated by the spin tensor $\mathbf{W}$, the resulting objective stress rate is called the *Jaumann stress rate*:

$$\tilde{\boldsymbol{\sigma}}^{\circ} = \dot{\boldsymbol{\sigma}} + \boldsymbol{\sigma} \cdot \mathbf{W} - \mathbf{W} \cdot \boldsymbol{\sigma} \tag{2.34}$$

The both above expressions remain objective even when these approximations do not apply ([3],[4]).

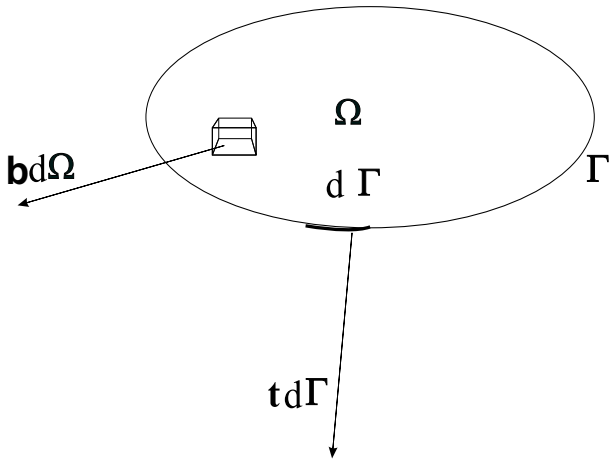

Figure 2.3: Body force and surface force

2.3 Motion and Equilibrium

2.3.1 Cauchy's Equation of Motion

The equations of motion are the key equations in finite element analysis. These equations emanate from the momentum conservation principle. Consider a body with the mass density ρ and with a volume Ω and a boundary Γ as shown in Fig. 2.3, under action of body forces $\mathbf{b}$ per unit volume and surface forces $\mathbf{t}$ per unit area. The total force $\mathbf{r}$ is then:

$$\mathbf{r} = \int_{\Gamma} \mathbf{t} d\Gamma + \int_{\Gamma} \mathbf{b} d\Omega \tag{2.35}$$

With the help of the definition of Cauchy stress and Gauss's divergence theorem, the first part of the right-hand side can be written as:

$$\int_{\Gamma} \mathbf{t} d\Gamma = \int_{\Gamma} \mathbf{n} \cdot \boldsymbol{\sigma} d\Gamma = \int_{\Omega} \nabla \cdot \boldsymbol{\sigma} d\Omega \tag{2.36}$$

Newton's second law of motion states that the material derivative of the linear momentum equals the total force, i.e.:

$$\frac{D(\int_{\Omega} \rho \boldsymbol{v} d\Omega)}{Dt} = \mathbf{r} \tag{2.37}$$

According to Reynolds' transport theorem and the mass conservation theorem:

$$\frac{D(\int_{\Omega} \rho \boldsymbol{v} d\Omega)}{Dt} = \int_{\Omega} \rho \frac{d(\boldsymbol{v})}{dt} d\Omega \tag{2.38}$$

Combine Eq. (2.35), Eq. (2.36) and Eq. (2.37), for an arbitrary volume Ω, at each point in this volume, the momentum balance is satisfied if:

$$\nabla \cdot \boldsymbol{\sigma} + \mathbf{b} = \rho \frac{d\boldsymbol{v}}{dt} \tag{2.39}$$

This is called Cauchy's first law of motion.

2.3.2 Equilibrium Equations

If the body is in equilibrium, the acceleration (the right-hand side of equation Eq. (2.39) will reduce to zero:

$$\nabla \cdot \boldsymbol{\sigma} + \mathbf{b} = 0 \tag{2.40}$$

This equilibrium equations apply to the current deformed configuration.

Above we pointed out the strains and stresses in different reference states. When the strains and stresses are defined in a reference state rather than the current state, the equations of motion in the reference state are needed. The equilibrium equations in the reference configuration are also derived from the external force in Ω. The body force in the initial volume is obtained from the body force $\mathbf{b}$ in the current configuration with $\mathbf{b}_0 = J\mathbf{b}$ as :

$$\mathbf{b} d\Omega = \mathbf{b} J d\Omega_0 = \mathbf{b}_0 d\Omega_0 \tag{2.41}$$

Using this form, the total force on the body is given in terms of the integral over the reference volume in the Lagrangian description and it will be equal to zero:

$$\int_{\Omega_0} \mathbf{b}_0(\mathbf{X}, t) d\Omega_0 + \int_{\Gamma_0} \mathbf{t}_0(\mathbf{X}, t) d\Gamma_0 = 0 \tag{2.42}$$

Using $\mathbf{n}_0 \cdot \mathbf{P} d\Gamma = \mathbf{t}_0 d\Gamma_0$ and Gauss's theorem, the second part of right-hand side of the equation above has the form:

$$\int_{\Omega_0} \mathbf{t}_0 d\Gamma_0 = \int_{\Gamma_0} \mathbf{n}_0 \cdot \mathbf{P} d\Gamma_0 = \int_{\Omega_0} \nabla_0 \cdot \mathbf{P} d\Omega_0 \tag{2.43}$$

So the equilibrium equation for the Lagrangian description is obtained in the first PK stress tensor form:

$$\nabla_0 \cdot \mathbf{P} + \mathbf{b}_0 = 0 \tag{2.44}$$

Substituting the definition of the second PK stress tensor into the equation above, the equilibrium equation for the second PK stress tensor becomes:

$$\nabla_0 \cdot [\mathbf{F} \cdot \mathbf{S}] + \mathbf{b}_0 = 0 \tag{2.45}$$

The motion and equilibrium equations together with their boundary conditions are called the strong form.

The finite element method was developed by introducing the weak form of these equations and boundary conditions. The procedure to derive the weak form of these equations is found in Chapter 4.

2.4 Constitutive Equations

The constitutive equations represent the mathematical description of material macroscopic behaviour resulting from the stress and strain of the material. In this section the emphasis is placed on elastic-plastic constitutive equations. The common forms of the Hypoelastic-plastic and Hyperelastic-plastic constitutive equations are discussed.

The plastic strain is defined as below. A material shows elastic and plastic deformation under loading. When the load is removed, the remaining strain is called the plastic strain. The stress state therefore becomes zero. The multiplicative decomposition of the deformation gradient $\mathbf{F}$ is the mathematical description for the statement above. An intermediate local configuration is introduced as a configuration, obtained from the current configuration by releasing stresses to the zero state or from the original configuration by plastic deformation. Therefore, the deformation of $d\mathbf{X}$ is deformed into $d\mathbf{x}^p$ by plastic flow:

$$d\mathbf{x}^p = \mathbf{F}^p \cdot d\mathbf{X} \tag{2.46}$$

where $\mathbf{F}^p$ is the plastic deformation gradient tensor. By elastic deformation, $d\mathbf{x}^p$ is then deformed into $d\mathbf{x}$ in the current configuration as follows:

$$d\mathbf{x} = \mathbf{F}^e \cdot d\mathbf{x}^p \tag{2.47}$$

Substituting these two equations into Eq. (2.4), the multiplicative decomposition of the deformation gradient tensor is formed as:

$$\mathbf{F} = \mathbf{F}^e \cdot \mathbf{F}^p \tag{2.48}$$

The velocity gradient $\mathbf{L}$ can be worked out as:

$$\mathbf{L} = \dot{\mathbf{F}} \cdot \mathbf{F}^{-1} = \dot{\mathbf{F}}^e \cdot (\mathbf{F}^e)^{-1} + \mathbf{F}^e \cdot \dot{\mathbf{F}}^p \cdot (\mathbf{F}^p)^{-1} \cdot (\mathbf{F}^e)^{-1} \tag{2.49}$$

$\mathbf{L}$ is split into elastic and plastic parts, i.e.,

$$\mathbf{L} = \mathbf{L}^e + \mathbf{L}^p \tag{2.50}$$

In this expression, $\mathbf{L}^e$ is the first term on the right-hand side and $\mathbf{L}^p$ is the second term on the right-hand side

$$\mathbf{L}^e = \dot{\mathbf{F}}^e \cdot (\mathbf{F}^e)^{-1} \tag{2.51}$$

and:

$$\mathbf{L}^p = \mathbf{F}^e \cdot \dot{\mathbf{F}}^p \cdot (\mathbf{F}^p)^{-1} \cdot (\mathbf{F}^e)^{-1} \tag{2.52}$$

where $\mathbf{L}^e$ and $\mathbf{L}^p$ can also be split into a symmetric part ($\mathbf{D}^e$ and $\mathbf{D}^p$) and an asymmetric part ($\mathbf{W}^e$ and $\mathbf{W}^p$):

$$\mathbf{L} = \mathbf{D}^e + \mathbf{W}^e + \mathbf{D}^p + \mathbf{W}^p \tag{2.53}$$

Therefore:

$$\mathbf{D} = \mathbf{D}^e + \mathbf{D}^p \tag{2.54}$$

$$\mathbf{W} = \mathbf{W}^e + \mathbf{W}^p \tag{2.55}$$

where $\mathbf{D}$ is the deformation rate tensor and $\mathbf{W}$ is the spin tensor.

2.4.1 Hypoelastic-plasticity

In hypoelastic-plastic material model a suitable objective rate of stress is a function of the elastic part of the deformation rate tensor $\mathbf{D}^e$. In pure elastic deformation, the stress rate is related to the total deformation-rate tensor:

$$\boldsymbol{\sigma}^{\triangledown} = \mathbf{C}_{el} \cdot \mathbf{D}^e = \mathbf{C}_{el} : (\mathbf{D} - \mathbf{D}^p) \tag{2.56}$$

Energy is not conserved in a close deformation for a hypoelastic material. But when the elastic deformation is very small, this energy error is insignificant([4]).

The general plastic flow theory includes a plastic flow rule, the yield function and a consistency condition. The evolution of plastic strains is governed by the plastic flow rule:

$$\mathbf{D}^p = \dot{\gamma}\mathbf{m}(\boldsymbol{\sigma}, \mathbf{q}) \tag{2.57}$$

Where $\dot{\gamma}$ is a scalar plastic flow rate and $\mathbf{m}$ is the plastic flow direction and is defined as:

$$\mathbf{m} = \frac{\partial \phi}{\partial \boldsymbol{\sigma}} \tag{2.58}$$

where ϕ is called the plastic flow potential. $\mathbf{q}$ is a set of internal variables.

The yield function is:

$$f(\boldsymbol{\sigma}, \mathbf{q}) = 0 \tag{2.59}$$

Evolution equations for the internal variables for most forms of plasticity are specified as:

$$\dot{\mathbf{q}} = \dot{\gamma}\mathbf{h}(\boldsymbol{\sigma}, \mathbf{q}) \tag{2.60}$$

For plastic behaviour not only the yield condition must hold, $f = 0$, but the plastic consistency condition must also be satisfied. The plastic consistency condition of Prager:

$$\dot{f} = 0 \tag{2.61}$$

restricts the stress path to remain on the yield surface.

The plastic rate parameter $\dot{\gamma}$ can be calculated from the consistency condition. f is the function of $\boldsymbol{\sigma}$ and $\mathbf{q}$, and by the chain rule the material time derivative of f is given as:

$$\dot{f} = \frac{\partial f}{\partial \boldsymbol{\sigma}} : \dot{\boldsymbol{\sigma}} + \frac{\partial f}{\partial \mathbf{q}} : \dot{\mathbf{q}} \tag{2.62}$$

In [4] the first term in the above equation can be rewritten as:

$$\frac{\partial f}{\partial \boldsymbol{\sigma}} : \dot{\boldsymbol{\sigma}} = \frac{\partial f}{\partial \boldsymbol{\sigma}} : \boldsymbol{\sigma}^{\triangledown} \tag{2.63}$$

Substitute Eq. (2.56) into Eq. (2.62) becomes:

$$\dot{f} = \frac{\partial f}{\partial \boldsymbol{\sigma}} : \mathbf{C}_{el} : (\mathbf{D} - \mathbf{D}^{p}) + \frac{\partial f}{\partial \mathbf{q}} : \dot{\mathbf{q}} = 0 \tag{2.64}$$

Using Eq. (2.57) and Eq. (2.60), Eq. (2.64) can be solved for $\dot{\gamma}$:

$$\dot{\gamma} = \frac{\frac{\partial f}{\partial \boldsymbol{\sigma}} : \mathbf{C}_{el} : \mathbf{D}}{-\frac{\partial f}{\partial \mathbf{q}} \cdot \mathbf{h} + \frac{\partial f}{\partial \boldsymbol{\sigma}} : \mathbf{C}_{el} : \mathbf{m}} \tag{2.65}$$

Substituting the above equation into Eq. (2.56) with Eq. (2.57), a relation between the objective rate of Cauchy stress and the total rate-of-deformation tensor is obtained:

$$\boldsymbol{\sigma}^{\triangledown} = \mathbf{C}_{el} : (\mathbf{D} - \dot{\gamma}\mathbf{m}) = \mathbf{C}_{t} : \mathbf{D} \tag{2.66}$$

The fourth-order tensor $\mathbf{C}_t$ is called the continuum elastic-plastic tangent modulus and is expressed as:

$$\mathbf{C}_{t} = \mathbf{C}_{el} - \frac{(\mathbf{C}_{el} : \mathbf{m}) \otimes (\frac{\partial f}{\partial \boldsymbol{\sigma}} : \mathbf{C}_{el})}{-\frac{\partial f}{\partial \mathbf{q}} \cdot \mathbf{h} + \frac{\partial f}{\partial \boldsymbol{\sigma}} : \mathbf{C}_{el} : \mathbf{m}} \tag{2.67}$$

2.4.2 Hyperelastic-plasticity

To avoid the drawback of the hypoelastic-plastic model, hyperelastic-plastic constitutive models were developed. First, hyperelastic materials are elastic materials for which the work is independent of load path, and are characterized by the stress, which is obtained from a stored energy function ψ ([3],[5]and [6]):

$$\mathbf{S} = 2\frac{\partial \psi(\mathbf{C}, \mathbf{C}^{p})}{\partial \mathbf{C}} \tag{2.68}$$

where ψ is the stored energy potential. There is no need for computing the stress using the stress rate equations (as in hypoelastic models). In terms of the variables $\mathbf{E}, \mathbf{E}^p$, $\mathbf{S}$ can also be described as:

$$\mathbf{S} = \frac{\partial \hat{\psi}(\mathbf{E}, \mathbf{E}^p)}{\partial \mathbf{E}} \tag{2.69}$$

In hyperelastic-plastic materials a multiplicative decompostion of the deformation gradient is applied:

$$\mathbf{F} = \mathbf{F}^e \cdot \mathbf{F}^p \tag{2.70}$$

$\mathbf{C}^p$ is defined as:

$$\mathbf{C}^p = \mathbf{F}^{pT} \cdot \mathbf{F}^p \tag{2.71}$$

$\mathbf{E}^p$ is therefore written as:

$$\mathbf{E}^p = \frac{1}{2}(\mathbf{C}^p - \mathbf{I}) \tag{2.72}$$

The yield condition in the material description is:

$$\phi(\mathbf{E}, \mathbf{E}^p, \mathbf{q}) \leq 0 \tag{2.73}$$

The evolution of the internal plastic variable vector $\mathbf{q}$ can also be written as:

$$\dot{\mathbf{q}} = \dot{\gamma}\mathbf{H}(\mathbf{E}, \mathbf{E}^p, \mathbf{q}) \tag{2.74}$$

Where $\mathbf{H}(\mathbf{E}, \mathbf{E}^p, \mathbf{q})$ is a prescribed function relating to the hardening or softening law. The plastic parameter $\dot{\gamma}$ is determined by the so-called consistency condition:

$$\dot{\gamma}\dot{\phi} = 0 \tag{2.75}$$

The plastic flow rule is obtained by the principle of maximum plastic dissipation (see the proof in [5]):

$$\frac{\partial^2 \hat{\psi}}{\partial \mathbf{E} \partial \mathbf{E}^p} : \dot{\mathbf{E}}^p = -\dot{\gamma}\frac{\partial \phi(\mathbf{E}, \mathbf{E}^p, \mathbf{q})}{\partial \mathbf{E}} \tag{2.76}$$

We assume:

$$\mathbf{M} = \frac{\partial^2 \hat{\psi}}{\partial \mathbf{E} \partial \mathbf{E}^p} \tag{2.77}$$

Eq. (2.76) has the form:

$$\mathbf{M} : \dot{\mathbf{E}}^p = -\dot{\gamma}\frac{\partial \phi(\mathbf{E}, \mathbf{E}^p, \mathbf{q})}{\partial \mathbf{E}} \tag{2.78}$$

$\mathbf{S}^p$ is defined from time differentiation of the expression for $\mathbf{S}$:

$$\dot{\mathbf{S}} = \frac{\partial \mathbf{S}}{\partial \mathbf{E}} : \dot{\mathbf{E}} + \frac{\partial \mathbf{S}}{\partial \mathbf{E}^p} : \dot{\mathbf{E}}^p := \mathbf{A} : \dot{\mathbf{E}} - \dot{\mathbf{S}}^p \tag{2.79}$$

Therefore, the plastic flow rule can be written as:

$$\dot{\mathbf{S}}^p = \dot{\gamma}\frac{\partial \phi}{\partial \mathbf{E}} \tag{2.80}$$

Eq. (2.73) can be worked out using the chain rule:

$$\dot{\phi}(\mathbf{E}, \mathbf{E}^p, \mathbf{q}) = \frac{\partial \phi}{\partial \mathbf{E}} : \dot{\mathbf{E}} + \frac{\partial \phi}{\partial \mathbf{E}^p} : \dot{\mathbf{E}}^p + \frac{\partial \phi}{\partial \mathbf{q}} : \dot{\mathbf{q}} = 0 \tag{2.81}$$

From this expression and Eqs. (2.79)and (2.80), $\dot{\gamma}$ is obtained:

$$\dot{\gamma} = \frac{\frac{\partial \phi}{\partial \mathbf{E}} : \dot{\mathbf{E}}}{\frac{\partial \phi}{\partial \mathbf{E}^p} : \mathbf{M}^{-1} : \frac{\partial \phi}{\partial \mathbf{E}} - \frac{\partial \phi}{\partial \mathbf{q}} : \mathbf{H}} \tag{2.82}$$

By substituting Eq. (2.82) and Eq.(2.80) into Eq. (2.79) the following expression is obtained:

$$\dot{\mathbf{S}} = (\mathbf{A} - \frac{\frac{\partial \phi}{\partial \mathbf{E}} \otimes \frac{\partial \phi}{\partial \mathbf{E}}}{\frac{\partial \phi}{\partial \mathbf{E}^p} : \mathbf{M}^{-1} : \frac{\partial \phi}{\partial \mathbf{E}} - \frac{\partial \phi}{\partial \mathbf{q}} : \mathbf{H}}) : \dot{\mathbf{E}} \tag{2.83}$$

Also, from Eq. (2.69):

$$\dot{\mathbf{E}}^p = -\mathbf{M}^{-1}(\frac{\frac{\partial \phi}{\partial \mathbf{E}} \otimes \frac{\partial \phi}{\partial \mathbf{E}}}{\frac{\partial \phi}{\partial \mathbf{E}^p} : \mathbf{M}^{-1} : \frac{\partial \phi}{\partial \mathbf{E}} - \frac{\partial \phi}{\partial \mathbf{q}} : \mathbf{H}})\dot{\mathbf{E}} \tag{2.84}$$

Here, we have obtained a similar form as that of the hypoelastic-plastic material model.

Bibliography

[1] Malveren, L.E.: Introduction to the mechanics of a continuous medium, Prentice-Hall, New York, 1969

[2] Zienkiewicz, O.C.: The finite element method (Third edition), Mcgraw-Hill Book Company (UK) Limited, 1979

[3] Bonet, J., Wood, R.D.: Nonlinear continuum mechanics for finite element analysis, Cambridge University Press, 1997

[4] Belytschko, T., Liu, W.K., Moran, B.: Nonlinear finite elements for continua and structures. John Wiley and Sons Ltd., England, 2001

[5] Simo, J.C.: A framework for finite strain elastoplasticity based on maximum plastic dissipation and the mulitplicative decomposition: part I. Continuum Formulation, Computer Methods in Applied Mechanics and Engineering, Vol 66, 199-219, 1988

[6] Simo, J.C., Hughes, T.J.R.: Computational inelasticity, Springer- Verlag, New York, Inc., 241-261 301-307, 1988

Chapter 3

Literature Review – Steady State

Start from the previous works

In this chapter a detailed review is made of literature on the modelling of steady state processes.The definition of a steady state is provided ed by means of mathematics and physics. First the common methods are discussed using the sources of previous works; Further on a referential steady state method has been presented by Balagangadhar([20−21]). This background and basic idea led to our research plan. The detailed project objective and problem definition have been written as the conclusions of this chapter.

3.1 Definition of a Steady State Process

In many forming processes such as extrusion, drawing, rolling, welding etc., the metal flows continuously. During these processes an invariant pattern of deformation develops (see Fig. 3.1). Hence the spatial distribution of the major field variables does not change with time during a steady state situation. The steady state characteristics should be expressed in a mathematical description so that these processes can be analyzed with numerical methods. For example, if an arbitrary history-dependent field variable, f, is expressed by either the referential or the spatial description:

$$f = \bar{f}(\mathbf{X}, t) = f(\boldsymbol{\phi}(\mathbf{X}, t), t) = f(\mathbf{x}, t) \tag{3.1}$$

The rate of change of f of a particle, the material time derivative (with the material coordinates $\mathbf{X}$ held constant), can be written in both a material (Lagrangian) and spatial (Eulerian) description:

$$\dot{f} = \frac{Df}{Dt} = \frac{\partial f}{\partial t}|_{\mathbf{X}} \quad \text{Lagrangian or material} \tag{3.2}$$

$$= \frac{\partial f}{\partial t}|_{\mathbf{x}} + \boldsymbol{v} \cdot \nabla_{\mathbf{x}} f \quad \text{Eulerian or spatial} \tag{3.3}$$

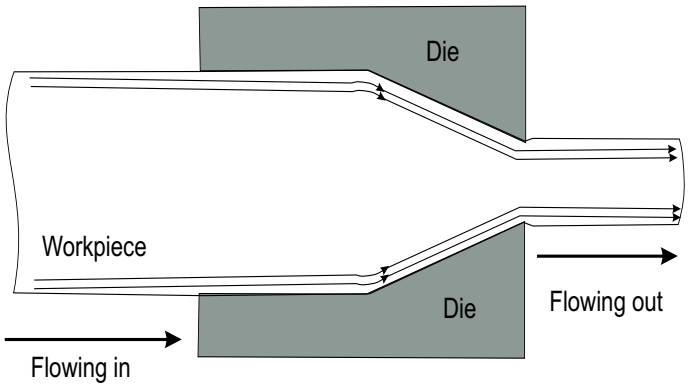

Figure 3.1: A steady state extrusion process

in which $\boldsymbol{v}$ is the velocity of a particle with material coordinates $\mathbf{X}$:

$$\boldsymbol{v} = \dot{\mathbf{x}} = \frac{\partial \mathbf{x}}{\partial t}|_{\mathbf{X}} \tag{3.4}$$

If we know only the expression of f in the spatial description and not under the material (referential) description, the rate of change of any material property may also be calculated from the spatial configuration, as long as $\boldsymbol{v}$ can be calculated.

The first term of the spatial description gives the local rate of change (local or spatial time derivative) of f. It is the rate of change which is observed at the fixed position $\mathbf{x}$; the second term gives the convective rate of change of f of a particle. In a steady flow, the local time derivative is zero everywhere, but the convective term may be nonzero. The reason is that the material property of a particle changes as it moves from one place to another place during flowing. In the steady flow, the streamline pattern is constant with time and each particle follows one of the unchanging streamlines.

Fig. 3.2 shows the characteristics of the steady state of a rolling process. When the steady state is reached at time t, the values of f which are measured at position $\mathbf{x}$ are the same from time t to a certain time t':

$$\frac{\partial f}{\partial t}|_{\mathbf{x}} = 0 \tag{3.5}$$

3.2 Steady State Formulations

The finite element method has been applied for simulating steady state metal forming processes during many years using different methods. There are three main formulations: Lagrangian, Eulerian, and the Arbitrary Lagrangian-Eulerian (ALE) method.

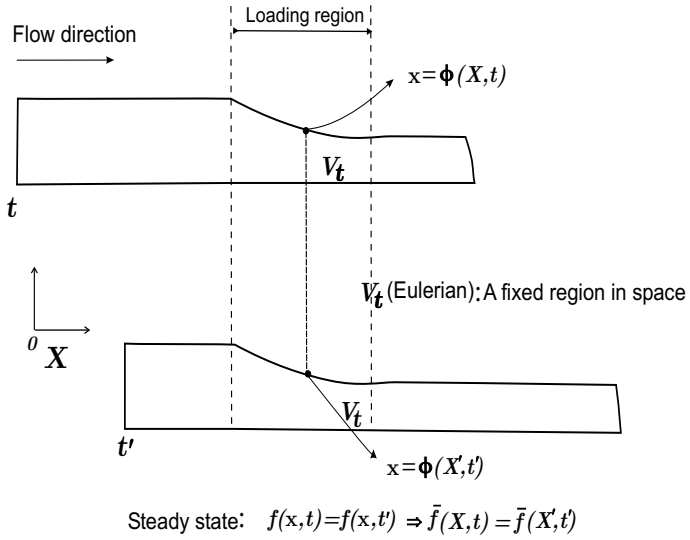

Figure 3.2: Physical characteristics of a steady rolling process

3.2.1 Lagrangian Formulation

In Lagrangian meshes, the nodes move with the material points. This means that the mesh motion coincides with the material motion. In solid mechanics this method is used. Since the mesh follows the material points, the history-dependent materials can be treated naturally ([23]), and free surface movement is automatically calculated. For example, the equations of conservation of mass in algebraic form are given simply by:

$$\rho J = \rho_0 \tag{3.6}$$

In which ρ represents the density of a material point and J is the Jacobian. There are two Lagrangian methods: the Updated Lagrangian(UL) and Total Lagrangian (TL) formulation. In UL, the strong form ([23]) is expressed in spatial coordinates, but in TL it is expressed in material, i.e. Lagrangian coordinates.

Use of the FE Lagrangian formulation started from the 1970s ([1]). The analysis is transient to calculate the evolution of the material state variables and terminates when the steady state is reached([2]−[5]). A large number of increments is needed to complete the whole process and the mesh includes a large upstream area so that the steady state situation can be reached([6],[7]). These disadvantages lead to increasing CPU time and computer storage. In addition, for history-dependent material, a time discretization is required in order to integrate an equation like Eq. (3.2). The interaction between the time and space discretizations can lead to numerical oscillations during

calculations ([1]). Due to the connection between the material points and the nodal points, the meshes follow the deformation of the material completely during the calculation, and become extremely distorted in the case of the large deformation.

3.2.2 Eulerian Formulation

In Eulerian meshes, the nodes and elements are fixed in space, so that the material flows through a fixed mesh ([8]∼[15]). This method is used often to simulate fluid mechanics problems, because the interest is normally concentrated on the spatial domain where the gradients in the flow patterns are large ([13]). The state variables are a function of the spatial coordinates and time, while the undeformed configuration does not exist. For example, the equation of conservation of mass has to be written as a partial differential equation rather than in algebraic form as in the Lagrangian formulation Eq. (3.6):

$$\frac{\partial \rho}{\partial t} + \frac{\partial (\rho \boldsymbol{v})}{\partial \mathbf{x}} = 0 \tag{3.7}$$

Similarly, the material derivatives of any state variable have the form as in Eq. (3.3).

In most cases the mesh is constructed according to the deformed shape. The boundary conditions are imposed on fixed mesh nodes. Hence, the problems are calculated on the whole domain at once, instead of using incremental steps as in a Lagrangian formulation. In order to obtain the material state variables (e.g. the stress or the cumulative plastic strain), integration of the evolution equations must be carried out along the unknown streamlines. Therefore, iterative techniques are required. One of the problems in this method is the free surface treatment, since the mesh has to be adjusted to make the surface a streamline ([11], [14] and [15]). In solid problems, Eulerian formulations have mostly been used for solving steady-state processes with rigid plastic material models.

3.2.3 ALE Formulation

During the last two decades a combined Lagrangian and Eulerian formulation called the Arbitrary Lagrangian-Eulerian (ALE) method has been developed to combine the advantages and solve the problems which occur in the above two traditional methods ([23]).

In an ALE method, the motion of the material is followed in the same way as Eq. (3.1). Another referential domain $\mathbf{V}_m$ is used to define the motion of the mesh. Assuming that χ are the ALE coordinates relating to the motion of the mesh, the mapping among three configurations is drawn in

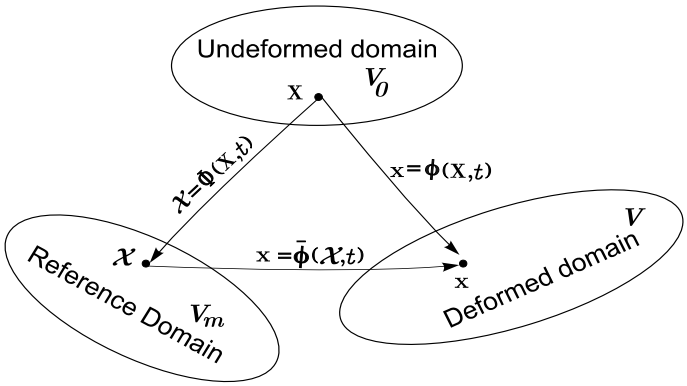

Figure 3.3: Mapping among Lagrangian, Eulerian and ALE

Fig. 3.3. The motion of the mesh is expressed by:

$$\mathbf{x} = \bar{\boldsymbol{\phi}}(\boldsymbol{\chi}, t) \tag{3.8}$$

In ALE the material motion can be obtained from the mesh motion using mapping, since:

$$\mathbf{x} = \boldsymbol{\phi}(\mathbf{X}, t) = \bar{\boldsymbol{\phi}}(\boldsymbol{\chi}, t) = \bar{\boldsymbol{\phi}}(\boldsymbol{\Phi}(\mathbf{X}, t), t) \tag{3.9}$$

with:

$$\boldsymbol{\chi} = \boldsymbol{\Phi}(\mathbf{X}, t) = \tilde{\boldsymbol{\phi}}(\mathbf{x}, t) \tag{3.10}$$

The mesh displacement $\bar{\mathbf{u}}$ is defined by:

$$\bar{\mathbf{u}} = \mathbf{x} - \boldsymbol{\chi} \tag{3.11}$$

The material derivative can be represented as a function of ALE coordinates $\boldsymbol{\chi}$ and time t in a similar process as that used in a Eulerian coordinate:

$$\dot{\breve{f}} = \dot{\breve{f}}(\boldsymbol{\chi}, t) = \frac{\partial \breve{f}(\boldsymbol{\chi}, t)}{\partial t}|_{\boldsymbol{\chi}} + \frac{\partial \breve{f}}{\partial \boldsymbol{\chi}} \frac{\partial \boldsymbol{\chi}}{\partial t}|_{\mathbf{x}} \tag{3.12}$$

Also, a chain rule expression can be developed for the material velocity:

$$\boldsymbol{v}_l = \frac{\partial \boldsymbol{\phi}}{\partial t}|_{\mathbf{x}} = \frac{\partial \bar{\boldsymbol{\phi}}}{\partial t}|_{\boldsymbol{\chi}} + \frac{\partial \bar{\boldsymbol{\phi}}(\boldsymbol{\chi}, t)}{\partial \boldsymbol{\chi}} \frac{\partial \boldsymbol{\chi}}{\partial t} = \boldsymbol{v}_e + \frac{\partial \bar{\boldsymbol{\phi}}(\boldsymbol{\chi}, t)}{\partial \boldsymbol{\chi}} \frac{\partial \boldsymbol{\chi}}{\partial t}|_{\mathbf{x}} \tag{3.13}$$

where $\boldsymbol{v}_l$ and $\boldsymbol{v}_e$ represent the material velocity and the mesh velocity, respectively. The referential velocity $\boldsymbol{w}$ is defined as:

$$\boldsymbol{v}_l = \boldsymbol{v}_e + \frac{\partial \mathbf{x}}{\partial \boldsymbol{\chi}} \boldsymbol{w} \tag{3.14}$$

Therefore we have:

$$\boldsymbol{w} = \frac{\partial \boldsymbol{\Phi}(\mathbf{X}, t)}{\partial t}|_{\mathbf{X}} \tag{3.15}$$

Substituting above two equations into Eq. (3.12):

$$\frac{Df}{Dt} = \frac{\partial \breve{f}(\boldsymbol{\chi}, t)}{\partial t}|_{\boldsymbol{\chi}} + \frac{\partial \breve{f}}{\partial \boldsymbol{\chi}}\boldsymbol{w} \tag{3.16}$$

$$= \frac{\partial \breve{f}(\boldsymbol{\chi}, t)}{\partial t}|_{\boldsymbol{\chi}} + \frac{\partial \breve{f}}{\partial \mathbf{x}}(\boldsymbol{v}_l - \boldsymbol{v}_e) = \frac{\partial \breve{f}(\boldsymbol{\chi}, t)}{\partial t}|_{\boldsymbol{\chi}} + \frac{\partial \breve{f}}{\partial \mathbf{x}}\boldsymbol{c} \tag{3.17}$$

with:

$$\boldsymbol{c} = \boldsymbol{v}_l - \boldsymbol{v}_e \tag{3.18}$$

In which the difference between the material and mesh velocities, $\mathbf{c}$, is called the convective velocity.

In a Eulerian formulation ($\boldsymbol{\chi} = \mathbf{x}$):

$$\boldsymbol{v}_e = 0 \qquad \boldsymbol{c} = \boldsymbol{v}_l \qquad \boldsymbol{w} = \boldsymbol{c} \tag{3.19}$$

In an updated Lagrangian formulation($\boldsymbol{\chi} = \mathbf{X}$):

$$\boldsymbol{v}_e = \boldsymbol{v}_l \qquad \boldsymbol{c} = \boldsymbol{w} = 0 \tag{3.20}$$

The equations of mass conservation Eq. (3.6) can be described in the ALE configuration via a transformation and will have the form:

$$\dot{\rho} + \rho \nabla_{\mathbf{x}} \cdot \boldsymbol{v}_l = 0 \tag{3.21}$$

Substituting Eq. (3.15) into the equations above:

$$\frac{\partial \breve{\rho}}{\partial t}|_{\boldsymbol{\chi}} + \boldsymbol{w}\frac{\partial \breve{\rho}_{\mathbf{x}}}{\partial \boldsymbol{\chi}} + \rho \nabla_{\mathbf{x}} \cdot \boldsymbol{v}_l = 0 \tag{3.22}$$

In this formulation the reference frame is associated neither with the material displacement as in the Lagrangian formulation nor fixed in space as in the Eulerian formulation. In this method the transient analysis is still required. At the same time, the free surface problem can be solved too. Since in ALE meshes the element coordinates are free from the material configuration, mesh distortion in the Lagrangian configuration can be prevented at a certain stage. However, handling the convective term could lead to spatial oscillations due to time discretizations and therefore the suitable discretization method must be taken into account. ALE has been successfully used for the simulation of steady state forming processes by a transient calculation until the processes are stationary([16]∼[19]).

3.3 Referential Formulation (Balagangadhar)

In 1998, D. Balagangadhar([20] and [21]) proposed his reference frame formulation for the simulation of steady state forming processes. His method concentrates on finding a referential coordinate by use of a mapping technique to eliminate the time effect in the convective equation (evolution equation). In this section we analyse his work.

3.3.1 Construction of a Reference Configuration

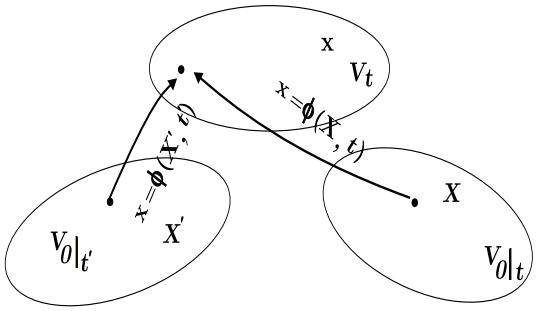

Figure 3.4: Relation between undeformed and deformed configurations

In Fig. 3.4, V_t represents the deformation region. At time t, V_t is the steady state deformed volume of a region V_0 in the undeformed configuration. Therefore:

$$V_t = \boldsymbol{\phi}(V_0, t) \tag{3.23}$$

Balagangadhar considers V_t as a fixed region in space, therefore V_0 changes with time:

$$V_0 = \boldsymbol{\phi}^{-1}(V_t, t) \tag{3.24}$$

A fixed reference configuration V_r is introduced (see Fig. 3.5). At any time t, V_0 is defined to be related to V_r by the mapping $\mathbf{g}$:

$$V_0 = \mathbf{g}(V_r, t) \tag{3.25}$$

Hence, position vectors $\mathbf{X}$ in V_0 can be described by $\mathbf{r}$ in V_r as:

$$\mathbf{X} = \mathbf{g}(\mathbf{r}, t) \tag{3.26}$$

Any state variables $\boldsymbol{f}$ can be expressed as $\bar{f}(\mathbf{X}, t)$ on V_0 and $\tilde{f}(\mathbf{r}, t)$ on V_r with equal values on both these two configurations at corresponding points:

$$\tilde{f}(\mathbf{r}, t) = \bar{f}(\mathbf{X}, t) = \bar{f}(\mathbf{g}(\mathbf{r}, t), t) \tag{3.27}$$

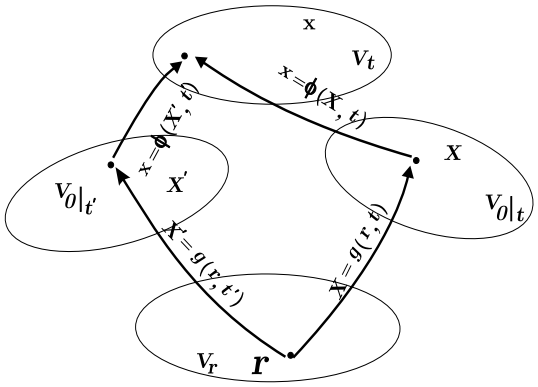

Figure 3.5: Relation among undeformed, deformed and referential configurations

The gradients and partial derivatives for the fields defined over both undeformed and reference configurations are defined as:

$$\nabla_{\mathbf{X}} \bar{f}(\mathbf{X}, t) = \frac{\partial \bar{f}}{\partial \mathbf{X}}(\mathbf{X}, t) \tag{3.28}$$

$$\nabla_{\mathbf{r}} \tilde{f}(\mathbf{r}, t) = \frac{\partial \tilde{f}}{\partial \mathbf{r}}(\mathbf{r}, t) \tag{3.29}$$

V_0 and V_r are related to each other by:

$$\mathbf{X} = \mathbf{r} + \boldsymbol{v}t \tag{3.30}$$

$\boldsymbol{v}$ is defined as the uniform inflow velocity and in fact V_0 is defined as the control volume of V_r when V_r moves to V_0 at time t with velocity $\boldsymbol{v}$.

3.3.2 Steady State at the Reference Configuration

According to the definition in Eq. (3.5), the steady state is reached when the local rate changes of parameters f become zero at the fixed position $\mathbf{x}$ in Eulerian coordinates (see Fig. 3.6), i.e.:

$$f(\mathbf{x}, t) = f(\mathbf{x}, t') \tag{3.31}$$

since the fixed position $\mathbf{x}$ can be described at any time (e.g. t and t' in the undeformed configuration:

$$\mathbf{x} = \boldsymbol{\phi}(\mathbf{X}, t) = \boldsymbol{\phi}(\mathbf{X}', t') \tag{3.32}$$

with:

$$f(\mathbf{x}, t) = f(\boldsymbol{\phi}(\mathbf{X}, t), t) = \bar{f}(\mathbf{X}, t) \tag{3.33}$$

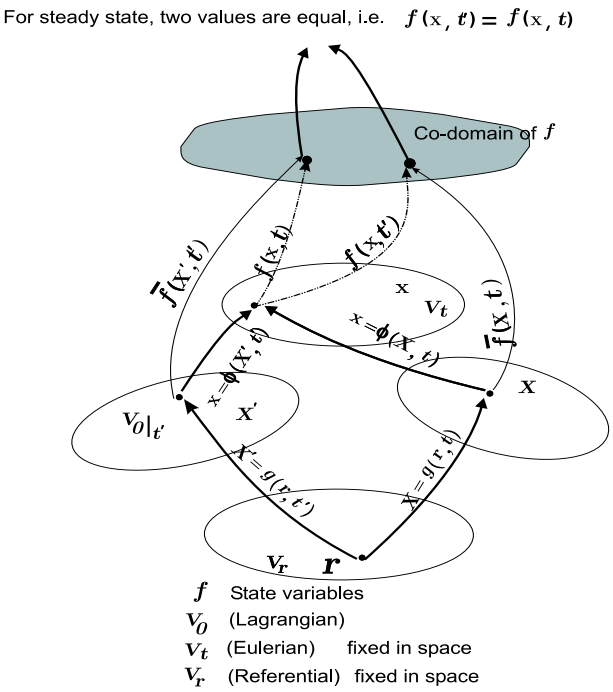

Figure 3.6: Physical explanation of steady state under undeformed and deformed configuration

$$f(\mathbf{x}, t') = f(\boldsymbol{\phi}(\mathbf{X}', t'), t') = \bar{f}(\mathbf{X}', t') \tag{3.34}$$

therefore, for steady state at any time:

$$\bar{f}(\mathbf{X}, t) = \bar{f}(\mathbf{X}', t') \tag{3.35}$$

Meanwhile the transformation can be made between the undeformed configuration V_0 and the referential configuration V_r by help of Eq. (3.26) and $\mathbf{X}' = \mathbf{g}(\mathbf{r}, t')$:

$$\bar{f}(\mathbf{X}, t) = \bar{f}(\mathbf{g}(\mathbf{r}, t), t) = \tilde{f}(\mathbf{r}, t) \tag{3.36}$$

and:

$$\bar{f}(\mathbf{X}', t') = \bar{f}(\mathbf{g}(\mathbf{r}, t'), t') = \tilde{f}(\mathbf{r}, t') \tag{3.37}$$

From Eq. (3.36), the steady state situation can be expressed for the referential configuration for any time (see Fig. 3.7):

$$\tilde{f}(\mathbf{r}, t) = \tilde{f}(\mathbf{r}, t') \tag{3.38}$$

i.e.:

$$\frac{\partial \tilde{f}}{\partial t}(\mathbf{r}, t) = 0 \tag{3.39}$$

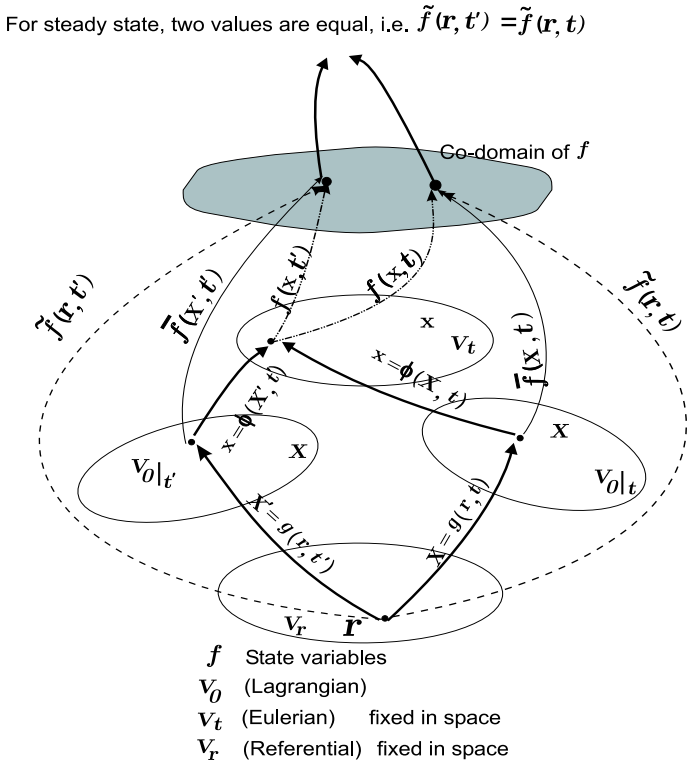

Figure 3.7: Physical explanation of steady state under reference configuration

When the process reaches steady state, the values of the state variables of points with the same fixed position $\mathbf{r}$ will be equal for any time.
Because of Eq. (3.26) and Eq. (3.36), for steady state there we have:

$$\frac{\partial \tilde{f}(\mathbf{r}, t)}{\partial t}|_{\mathbf{r}} = \frac{\partial \bar{f}(\mathbf{X}, t)}{\partial t}|_{\mathbf{X}} + \frac{\partial \bar{f}(\mathbf{X}, t)}{\partial \mathbf{X}} \frac{\partial \mathbf{g}(\mathbf{r}, t)}{\partial t}|_{\mathbf{r}} = 0 \tag{3.40}$$

or:

$$\dot{\bar{f}} = \frac{\partial \bar{f}(\mathbf{X}, t)}{\partial t}|_{\mathbf{X}} = \frac{\partial \tilde{f}(\mathbf{r}, t)}{\partial t}|_{\mathbf{r}} + \frac{\partial \tilde{f}(\mathbf{r}, t)}{\partial \mathbf{r}} \frac{\partial \mathbf{r}}{\partial t}|_{\mathbf{X}} \tag{3.41}$$

Using the chain rule:

$$\frac{\partial \bar{f}(\mathbf{X}, t)}{\partial \mathbf{X}} = \frac{\partial \tilde{f}(\mathbf{r}, t)}{\partial \mathbf{r}} \frac{\partial \mathbf{r}}{\partial \mathbf{X}} = \frac{\partial \tilde{f}(\mathbf{r}, t)}{\partial \mathbf{r}} \mathbf{F}_r \tag{3.42}$$

where $\mathbf{F}_r$ is the transformation tensor between the undeformed configuration and the reference configuration. Eq. (3.40) can therefore be rewritten as:

$$\frac{\partial \bar{f}(\mathbf{X}, t)}{\partial t}|_{\mathbf{X}} = -\frac{\partial \tilde{f}(\mathbf{r}, t)}{\partial \mathbf{r}} \frac{\partial \mathbf{r}}{\partial \mathbf{X}} \frac{\partial \mathbf{g}(\mathbf{r}, t)}{\partial t}|_{\mathbf{r}} \tag{3.43}$$

Eq. (3.41) gives the form in steady state because of Eq. (3.39):

$$\dot{\bar{f}} = \frac{\partial \bar{f}(\mathbf{X}, t)}{\partial t}|_{\mathbf{X}} = \frac{\partial \tilde{f}(\mathbf{r}, t)}{\partial \mathbf{r}} \frac{\partial \mathbf{r}}{\partial t}|_{\mathbf{X}} \tag{3.44}$$

This gives the same result as in Eq. (3.43), due to:

$$\frac{\partial \mathbf{r}}{\partial t}|_{\mathbf{X}} + \frac{\partial \mathbf{r}}{\partial \mathbf{X}} \frac{\partial \mathbf{g}(\mathbf{r}, t)}{\partial t}|_{\mathbf{r}} = 0 \tag{3.45}$$

The proof can be found in Appendix *A*.

The expression Eq. (3.43) shows that in steady state the material derivative only depends on the gradient of $\mathbf{f}$ under the reference configuration $\mathbf{r}$, $\mathbf{F}_r$ and $\frac{\partial \mathbf{g}(\mathbf{r},t)}{\partial t}$ (i.e. $\dot{\mathbf{g}}|_{\mathbf{r}} = \mathbf{v}$). Since $\mathbf{F}_r$ is defined on the basis of the transformation between the undeformed field and the reference configuration, the material derivative can be obtained via the gradient of the reference fields. In conclusion, the reference fields do not vary in time in the reference configuration. This result can be used to obtain the material derivatives without applying time differentiation.

3.3.3 Contact Problem

Balagangadhar made several assumptions:

1. The tool is rigid.
2. The contact surface is smooth.
3. The contact surface ∂V_r^c in the reference configuration is treated as a priori.
4. The Coulomb friction model is applied.
5. The normal traction over the boundary of the contact area is zero (an equality contact constraint, unlike in Lagrangian analysis an inequality constraint).

The last item aims to obtain the contact area in the undeformed configuration because the location of the contact area is unknown. An additional response field $\boldsymbol{\alpha}$ has to be introduced in the relation between the initial and referential configurations. The mapping $\mathbf{X} = \mathbf{g}(\mathbf{r}, t, \boldsymbol{\alpha})$ is defined to divide several flexible subregions in order to satisfy the 5^{th} assumption.

It is found that $\mathbf{F}_r$ is no longer a unit tensor as in the non-contact situation. But it still only depends on the element lengths of the undeformed and reference configurations.

3.3.4 Solution Procedure

The momentum balance equations represented by the second PK stress tensor are:

$$\nabla_0 \cdot (\mathbf{FS}) + \mathbf{b} = \mathbf{0} \tag{3.46}$$

The momentum balance equations can be transformed from these equations:

$$\nabla_{\mathbf{r}} \cdot (J\mathbf{FSF}_r) + J\mathbf{b} = 0 \tag{3.47}$$

Furthermore, the evolution equations in the reference configuration, using the consistency conditions, can be described as:

$$\dot{\mathbf{C}}^p = \Theta(\dot{\mathbf{C}}, \mathbf{C}, \mathbf{Q}) \tag{3.48}$$

in which $\mathbf{Q}$ represents other variables.

For steady state, due to Eq. (3.42), the material derivatives are:

$$\dot{\mathbf{C}}^p = -\frac{\partial \tilde{\mathbf{C}}^p(\mathbf{r}, t)}{\partial \mathbf{r}} \mathbf{F}_r(\mathbf{r}, t) \frac{\partial \mathbf{g}}{\partial t} \tag{3.49}$$

Using the integration technique, $\mathbf{C}^p$ can obtained directly without time integration. The streamline Upwind Petrov-Galerkin method is applied for reducing the numerical instabilities when solving the material evolution equations.

Balagangadhar used the coupled methods to solve the above three equations using FEM. The stress can be calculated with the hyperelastic model with linear isotropic hardening, since this model provides a direct relation between stress and strain.

3.3.5 Remarks

Some remarks are made concerning the work of Balagangadhar:

1. A transient analysis is not required, as the reference fields do not vary in time in the steady state situation. The displacements and plastic strains are the primary variables.

2. Elastic spring-back can be obtained directly because the plastic parameter can be calculated from its rate form.

3. The material evolution equations in the reference configuration are similar to those in the Eulerian configuration. Integration of these equations does not require time integration, since these equations are dependent only of inflow velocity and the undeformed contact region. Therefore the integration of the material evolution equations was carried out along the known streamlines.

4. The contact problem cannot be treated as in the conventional Lagrangian, Eulerian and ALE formulations.

5. A mathematical coordinate transformation is required to obtain the reference configuration, which makes the procedure complicated and more difficult to understand.

3.4 Objectives of This Project

Balagangadhar's work opens a new field for modelling steady state flow problems. The objectives of our project were:

1. To find a simple definition of the evolution equations based on the undeformed configuration. Balagangadhar's referential configuration was too complicated for use in practical situations.

2. To use a different solution methodology and numerical techniques.

3. To obtain more insight into steady state process modelling.

Bibliography

[1] Lee, E.H., Mallett, R.L., and Yang, W.H.: Stress and deformation analysis of the metal extrusion processes. Computer Methods in Applied Mechanics Engineering. Vol. 10, 1977, 339-353

[2] Appleby, E., Lu, Y., Rao, R.S., Devenpeck, M.L., Wright, P.K., and Richmond, O.: Strip drawing: A theoretical-experimental comparison. International Journal of Mechanical Sciences. Vol. 26, No.5, 1984, 351-362

[3] Liu, C., Hartley, P., Sturgess, C., Rowe, W.: Elastic-plastic finite-element modelling of cold rolling of strip. International Journal of Mechanical Sciences. Vol. 27, No.7/8, 1985, 531-541

[4] Carroll III, J.T., Strenkowski, J.S.: Finite element models of orthogonal cutting with application to single point diamond turning. International Journal of Mechanical Sciences. Vol.30, No.12, 1988, 899-920

[5] Suh, Y.S., Agah-Tehrani, A., Chung, K.: Stress analysis of axisymmetric extrusion in the presence of strain-induced anisotropy models as combined isotropic-kinematic hardening. Computer Methods in Applied Mechanics and Engineering. Vol. 93, 1991, 127-150

[6] Rowe, G.W., Sturgess, C.E.N., Hartley, P., Pillinger, I.: Finite-element plasticity and metalforming analysis. Cambridge University Press, 1991

[7] Gouveia, B.P.P.A., Rodrigues, J.M.C., and Martins, P.A.F.: Steady-state finite element analysis of cold forward extrusion. Journal Material Processing Technology. Vol. 73, 1998, 281-288

[8] Dawson, P., R., Thompson, E., G.: Finite element analysis of steady-state elasto-visco-plastic flow by the initial stress-rate method, International Journal for Numerical Methods in Engineering. Vol.12, 1978, 47-57

[9] Abo-elkhier, M., Oravas, G.A., and Dokainish, M.A.: A consistent Eulerian formulation for large deformation analysis with reference to metal-extrusion process. International Journal of Non-Linear Mechanics. Vol 23, No.1 1988, 37-52

[10] Yu,S.W. , Thompson, E.: A direct Eulerian finite element method for steady state elastic plastic flow. NUMIFORM 89, Thompson et al. (eds),

Balkema, Rotterdam, 1989,95-103
[11] Thompson, E.G., Yu, S.W.: A flow formulation for rate equilibrium equations. International Journal for Numerical Methods in Engineering. Vol. 30, 1990, 1619-1632
[12] Maniatty, A., M., Dawson, P., R., Weber, G., G.: An Eulerian elastic-viscoplastic formulation for steady-state forming processes, International Journal of Mechanical Sciences. Vol. 33, No.5, 1991, pp.361-377
[13] Legat, V., Marchal, J. M.: Prediction of three-dimensional general shape extrudates by an implicit iterative scheme. International Journal for Numerical Methods in Fluids. Vol. 14, No.1, 1992, 609-625
[14] Lefebvre, L., Keunings, R.: Finite element modelling of the flow of chemically reactive polymeric liquids. IInternational Journal for Numerical Methods in Fluids. Vol. 20, 1995, 319-334
[15] Ramanan, N., Engelman, M.S.: An algorithm for simulation of steady free surface flows. International Journal for Numerical Methods in Fluids. Vol. 22, 1996, 103-120
[16] Malinowski, Z., Lenard, J., G.: Experimental substantiation of an elastoplastic finite element scheme for flat rolling, omputer Methods in Applied Mechanics Engineering. 1993, 1-17
[17] Hu, Y.K. , Liu., W.K.: An ALE hydrodynamic lubrication finite element method with application to strip rolling. International Journal for Numerical Methods in Engineering. Vol. 36, 1993, 855-880
[18] Huétink, J.: On the simulation of thermo-mechanical forming processes - A mixed Eulerian-Lagrangian finite element method, Ph.D thesis, University of Twente, Enschede, The Netherlands, 1986
[19] Wisselink, H.: Analysis of guillotining and slitting - finite element simulations, PhD thesis, University of Twente, Enschede, The Netherlands, 2000, 33-48
[20] Balagangadhar, D., Tortorelli,D.A. Design of large-deformation steady elastoplastic manufacturing processes. Part I: a displacement-based reference frame formulation. International Journal for Numerical Methods in Engineering. Vol. 49, 2000, 899-932
[21] Balagangadhar, D., Dorai, G.A., Tortorelli, D.A.: A displacement-based reference frame formulation for steady-state thermo-elasto-plastic material processes. International Journal of Solids Structures. Vol. 36, 1999, 2397-2416
[22] Malvern, L., E.,: Introduction to the mechanics of a continuous medium, Prentice-Hall, New York, 1969
[23] Belytschko, T., Liu, W.K., Moran, B.: Nonlinear finite elements for continua and structures. John Wiley and Sons Ltd., England, 2001

Chapter 4

Finite Element Method

Stepping stone to structure modelling

Some simulations of the mechanical processes have already been carried out based on the finite element method. This method aims to find the numerical solutions for the motion equation together with the boundary conditions. The essence of this method is to obtain the weak form of the momentum equations (strong form) with the help of the principle of virtual work. In this chapter, the relationship between the weak form and the strong form is discussed. Secondly, the finite element method procedure is introduced by the linearization, FE discretization and iterative solution procedure, step by step.

4.1 Principle of Virtual Work

Assume a body is in a certain equilibrium state with the boundary conditions:

$$\mathbf{u} = \bar{\mathbf{u}} \quad \text{on } \Gamma_u \tag{4.1}$$

$$\mathbf{t} = \bar{\mathbf{t}} \quad \text{on } \Gamma_t \tag{4.2}$$

and give every point of the body an infinitesimal virtual displacement $\delta\mathbf{u}_i$ from the equilibrium configuration. These virtual displacement (or velocity) functions are called the test functions. The space of these functions are defined by:

$$\delta\mathbf{u}_i \in \Pi \qquad \Pi = \{\delta\mathbf{u}_i | \delta\mathbf{u}_i \in C^0, \delta\mathbf{u}_i = \mathbf{0} \qquad \text{on } \Gamma_u\} \tag{4.3}$$

A function is C^n continuous, if the nth derivative of this function is a continuous function.

The virtual work of the static spatial equilibrium equations Eq. (2.40) of one point in the body is represented as follows:

$$\delta w = \delta \mathbf{u} \cdot (\nabla \cdot \boldsymbol{\sigma} + \mathbf{b}) = 0 \tag{4.4}$$

We integrate over the volume of the body to obtain the virtual work of the body in the equilibrium state:

$$\delta W = \int_{\Omega} \delta \mathbf{u} \cdot (\nabla \cdot \boldsymbol{\sigma} + \mathbf{b}) d\Omega = 0 \tag{4.5}$$

Applying the divergence theorem:

$$\nabla \cdot (\delta \mathbf{u} \cdot \boldsymbol{\sigma}) = \boldsymbol{\sigma} : (\nabla \delta \mathbf{u}) + \delta \mathbf{u} \cdot (\nabla \cdot \boldsymbol{\sigma}) \tag{4.6}$$

Eq. (4.5) has the form:

$$\delta W = \int_{\Omega} [\nabla \cdot (\delta \mathbf{u} \cdot \boldsymbol{\sigma}) - \boldsymbol{\sigma} : (\nabla \delta \mathbf{u} + \delta \mathbf{u} \cdot \mathbf{b})] d\Omega = 0 \tag{4.7}$$

Together with Gauss theorem the equation above can be rewritten as:

$$\delta W = \int_{\Gamma_t} \delta \mathbf{u} \boldsymbol{\sigma} \cdot \mathbf{n} d\Gamma - \int_{\Omega} \nabla \delta \mathbf{u} : \boldsymbol{\sigma} d\Omega + \int_{\Omega} \delta \mathbf{u} \cdot \mathbf{b} d\Omega = 0 \tag{4.8}$$

in which:

$$\nabla \delta \mathbf{u} = \delta \boldsymbol{\varepsilon} + \delta \boldsymbol{\omega} \tag{4.9}$$

with the virtual strain and rotation tensor, respectively:

$$\delta \boldsymbol{\varepsilon} = \frac{1}{2} (\nabla \mathbf{u} + (\nabla \mathbf{u})^T) \tag{4.10}$$

and:

$$\delta \boldsymbol{\omega} = \frac{1}{2} (\nabla \mathbf{u} - (\nabla \mathbf{u})^T) \tag{4.11}$$

Because $\delta \boldsymbol{\omega}$ is skew-symmetric and $\boldsymbol{\sigma}$ is symmetric:

$$\nabla \delta \mathbf{u} : \boldsymbol{\sigma} = \delta \boldsymbol{\varepsilon} : \boldsymbol{\sigma} + \delta \boldsymbol{\omega} : \boldsymbol{\sigma} = \delta \boldsymbol{\varepsilon} : \boldsymbol{\sigma} \tag{4.12}$$

With $\mathbf{t} = \boldsymbol{\sigma} \cdot \mathbf{n}$, finally, the spatial virtual work equation is expressed as:

$$\delta W = - \int_{\Omega} \delta \boldsymbol{\varepsilon} : \boldsymbol{\sigma} d\Omega + \int_{\Gamma_t} \delta \mathbf{u} \cdot \mathbf{t} d\Gamma + \int_{\Omega} \delta \mathbf{u} \cdot \mathbf{b} d\Omega = 0 \tag{4.13}$$

The proof that the weak form implies the strong form can be found in the literature ([1],[8]).

The virtual work equations in the reference states can be obtained in

terms of the different material stress tensors, which are introduced in Chapter 2.

Following a similar derivation, the weak form of the equilibrium equation based on the first PK stress tensor can be written as:

$$\delta W = -\int_{\Omega_0} \nabla_0 \delta \mathbf{u} : \mathbf{P} d\Omega_0 + \int_{\Gamma_t} \delta \mathbf{u} \cdot \mathbf{t}_0 d\Gamma_0 + \int_{\Omega_0} \delta \mathbf{u} \cdot \mathbf{b}_0 d\Omega_0 = 0 \tag{4.14}$$

because $\mathbf{u} = \mathbf{x} - \mathbf{X}$ and therefore $\delta \mathbf{u} = \delta \mathbf{x}$. Hence ([8]):

$$\nabla_0 \delta \mathbf{u} : \mathbf{P} = \delta \mathbf{F}^T : \mathbf{P} \tag{4.15}$$

Eq. (4.14) is rewritten as:

$$\int_{\Omega_0} \delta \mathbf{F}^T : \mathbf{P} d\Omega_0 - \int_{\Gamma_t} \delta \mathbf{u} \cdot \mathbf{t}_0 d\Gamma_0 - \int_{\Omega_0} \delta \mathbf{u} \cdot \mathbf{b}_0 d\Omega_0 = 0 \tag{4.16}$$

The weak form in terms of the second PK stress tensor can be obtained from the equation above. The second and third terms are similar, and only the first term need be worked out. Using Eq. (2.23) this term becomes:

$$\int_{\Omega_0} \delta \mathbf{F}^T : (\mathbf{F} \cdot \mathbf{S}) d\Omega_0 \tag{4.17}$$

because:

$$\mathrm{tr}(\delta \mathbf{F}^T \cdot \mathbf{F} \cdot \mathbf{S}) = \mathrm{tr}(\mathbf{F}^T \cdot \delta \mathbf{F} \cdot \mathbf{S}^T) \tag{4.18}$$

With $\mathbf{S}^T = \mathbf{S}$ we have:

$$\mathrm{tr}(\delta \mathbf{F}^T \cdot \mathbf{F} \cdot \mathbf{S}) = \mathrm{tr}(\mathbf{F}^T \cdot \delta \mathbf{F} \cdot \mathbf{S}) = \frac{1}{2}(\delta \mathbf{F}^T \cdot \mathbf{F} + \mathbf{F}^T \cdot \delta \mathbf{F}) : \mathbf{S} \tag{4.19}$$

Then:

$$\delta \mathbf{F}^T : (\mathbf{F} \cdot \mathbf{S}) = \frac{1}{2}(\delta \mathbf{F}^T \cdot \mathbf{F} + \mathbf{F}^T \cdot \delta \mathbf{F}) : \mathbf{S} \tag{4.20}$$

Taking the virtual rate of the right Cauchy-Green tensor $\mathbf{C} = \mathbf{F}^T \mathbf{F}$:

$$\delta \mathbf{C} = \delta \mathbf{F}^T \cdot \mathbf{F} + \mathbf{F}^T \cdot \delta \mathbf{F} \tag{4.21}$$

Therefore,

$$\int_{\Omega_0} \nabla_0 \delta \mathbf{u} : (\mathbf{F} \cdot \mathbf{S}) d\Omega_0 = \int_{\Omega_0} \frac{1}{2} \delta \mathbf{C} : \mathbf{S} d\Omega_0 \tag{4.22}$$

The weak form of the equilibrium equations in terms of the second PK stress tensors has the form:

$$\delta W = -\int_{\Omega_0} \delta \mathbf{E} : \mathbf{S} d\Omega_0 + \int_{\Gamma_t} \delta \mathbf{u} \cdot \mathbf{t}_0 d\Gamma_0 + \int_{\Omega_0} \delta \mathbf{u} \cdot \mathbf{b}_0 d\Omega_0 = 0 \tag{4.23}$$

4.2 Linearization of the Weak Form

In general, the virtual work expression of the equilibrium equations is nonlinear with respect to the material and the geometry. In order to solve these nonlinear equations in the finite element method, a Newton-Raphson iterative solution is used. Hence, the linearization of the weak form of the equilibrium equations is required. In this part the linearization procedure is described with respect to the material description of the equilibrium equations Eq. (4.23).

First here the directional derivative is introduced. The directional derivative represents the gradient of the potential energy function $\prod$ in the direction of an incremental displacement $\mathbf{u}$:

$$D\prod(\mathbf{x})[\mathbf{u}] \approx \prod(\mathbf{x}+\mathbf{u}) - \prod(\mathbf{x}) \tag{4.24}$$

where $D\prod(\mathbf{x})[\mathbf{u}]$ gives a linear approximation to the increment in the potential energy due to the increment in position $\mathbf{u}$.

Let us consider the solution of a set in the nonlinear weak form,

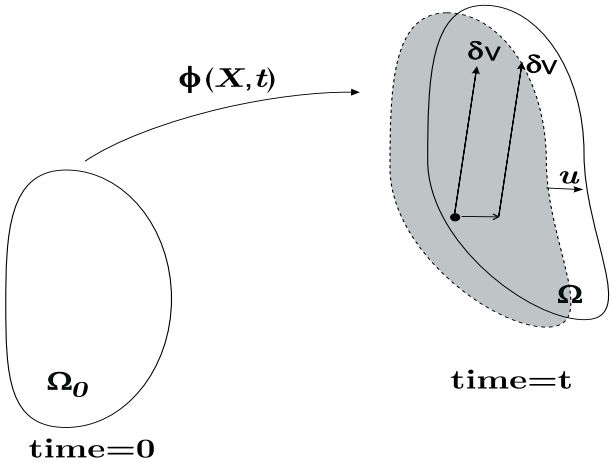

Figure 4.1: Linearized equilibrium

$$\delta W(\boldsymbol{\varphi}, \delta\mathbf{u}) = 0 \tag{4.25}$$

where $\boldsymbol{\varphi}$ is the solution of the equilibrium state. Consider a trial solution $\boldsymbol{\varphi}_t$, the above equations can be linearized if the equilibrium state is satisfied. Then:

$$\delta W(\boldsymbol{\varphi}_t + \mathbf{u}, \delta\mathbf{u}) \approx \delta W(\boldsymbol{\varphi}_t, \delta\mathbf{u}) + D\delta W(\boldsymbol{\varphi}_t, \delta\mathbf{u})[\mathbf{u}] = 0 \tag{4.26}$$

The virtual displacement $\delta\mathbf{u}$ does not alter during the incremental change $\mathbf{u}$ (see Fig. 4.1).

The linearization of the virtual work can be split into two parts: the internal and external virtual work components according to Eq. (4.23):

$$D\delta W(\boldsymbol{\varphi}_t, \delta\mathbf{u})[\mathbf{u}] = D\delta W_{in}(\boldsymbol{\varphi}_t, \delta\mathbf{u})[\mathbf{u}] - D\delta W_{ex}(\boldsymbol{\varphi}_t, \delta\mathbf{u})[\mathbf{u}] \tag{4.27}$$

where:

$$\delta W_{in} = \int_{\Omega_0} \delta\mathbf{E} : \mathbf{S} d\Omega_0 \tag{4.28}$$

and:

$$\delta W_{ex} = \int_{\Omega_0} \delta\mathbf{u} \cdot \mathbf{b} d\Omega + \int_{\Gamma_0} \delta\mathbf{u} \cdot \mathbf{t} d\Gamma \tag{4.29}$$

First the directional derivative of the internal virtual work is obtained:

$$\begin{aligned} D\delta W_{in}[\mathbf{u}] &= D(\int_{\Omega_0} (\delta\mathbf{E} : \mathbf{S})[\mathbf{u}] d\Omega_0) \\ = \int_{\Omega_0} \delta\mathbf{E} : D\mathbf{S}[\mathbf{u}] d\Omega_0 &+ \int_{\Omega_0} \mathbf{S} : D\delta\mathbf{E}[\mathbf{u}] d\Omega_0 \end{aligned} \tag{4.30}$$

Because of the constitution relation between the stresses and the strains:

$$D\mathbf{S}[\mathbf{u}] = \frac{\partial \mathbf{S}}{\partial \mathbf{E}} : D\mathbf{E}[\mathbf{u}] = \mathbf{C}_e : D\mathbf{E}[\mathbf{u}] \tag{4.31}$$

where $\mathbf{C}_e$ is called the tangent modulus tensor.

The term $D\delta\mathbf{E}[\mathbf{u}]$ can be worked out from:

$$\delta\mathbf{E} = \frac{1}{2}(\delta\mathbf{F}^T \cdot \mathbf{F} + \mathbf{F}^T \cdot \delta\mathbf{F}) \tag{4.32}$$

with:

$$\delta\mathbf{F} = (\nabla_0 \delta\mathbf{u})^T \tag{4.33}$$

and:

$$D\mathbf{F}[\mathbf{u}] = (\nabla_0 \mathbf{u})^T \tag{4.34}$$

Because $\nabla_0\delta\mathbf{u}$ is constant as it is independent both of configuration and the symmetry of $\mathbf{S}$, the result can be expressed as:

$$\begin{aligned} \mathbf{S} : D\delta\mathbf{E}[\mathbf{u}] = \mathbf{S} : \frac{1}{2}[\nabla_0\delta\mathbf{u} \cdot (\nabla_0\mathbf{u})^T + \nabla_0\mathbf{u} \cdot (\nabla_0\delta\mathbf{u})^T] \\ = \mathbf{S} : [(\nabla_0\mathbf{u})^T \cdot \nabla_0\delta\mathbf{u}] \end{aligned} \tag{4.35}$$

Substituting Eq. (4.35) into Eq. (4.30), the directional derivative of the internal virtual work has the form:

$$D\delta W_{in} = \int_{\Omega_0} \delta\mathbf{E} : \boldsymbol{C}_e : D\mathbf{E}[\mathbf{u}] d\Omega_0 + \int_{\Omega_0} \mathbf{S} : [(\nabla_0\mathbf{u})^T \nabla_0\delta\mathbf{u}] d\Omega_0 \tag{4.36}$$

The body force and the surface force contribute to the external forces. The directional derivatives of both external virtual work terms are considered separately. One of the most common body forces is self-weight or gravity loading with $\mathbf{b} = \rho_0 \mathbf{g}$ in the initial state. The virtual work of the body force is therefore given as:

$$\delta W_{ex}(\boldsymbol{\varphi}, \delta\mathbf{u}) = \int_{\Omega_0} \rho_0 \mathbf{g} \cdot \delta\mathbf{u} d\Omega \tag{4.37}$$

Because the terms in the above equation are independent of the current state and by definition $D\delta\mathbf{u}[\mathbf{u}] = 0$, then:

$$D\delta W_{ex}(\boldsymbol{\varphi}, \delta\mathbf{u}) = 0 \tag{4.38}$$

The friction contact is the most common cause of surface traction, and its linearization is complex. In this section it will not be discussed further and the surface traction is assumed to be zero. The issue about the contact force will be discussed in Chapter 5, where the contact analysis is discussed for this case.

It is found that the equilibrium equations and their corresponding linearizations have the integration forms. As a consequence, the finite element method has been developed to deal with these problems. Besides linearization of the weak form as one of the main steps in the finite element method, there are three important procedures in this method: finite element discretization, approximation to integral formulations (weighted residuals), and the iteration solution procedure (Newton-Raphson method). In the next section, finite element discretization is discussed together with the Galerkin weighted method. Furthermore, after having obtained the discretized equilibrium equations, the solution of these equations was carried out via iterative methods, for example, Newton-Raphson method.

4.3 Finite Element Discretization

In the finite element method the domain Ω is divided into subdomains Ω_e, which are called elements, so that:

$$\Omega = \cup\Omega_e \tag{4.39}$$

These elements are defined by means of nodes. The independent variables are calculated in these nodes and they reprensent the degrees of freedom (dof) system. The node coordinates in the current configuration can be denoted by x_{iI}, where I is the nodal number and i is the degree of freedom, such that $x_{iI} = [x_I, y_I]$. The nodal coordinates in the initial state are denoted by X_{iI}. The discretization is established using the elements to

interpolate the quantities or geometry in terms of the nodal values in the initial configuration:

$$X_i = N_I(\boldsymbol{\xi})X_{iI} \qquad \text{or} \qquad \mathbf{X} = N_I(\boldsymbol{\xi})\mathbf{X}_I \tag{4.40}$$

In the following discussion the second representation is chosen for simplicity. Similarly, the motion can be fully described by means of the current position $\mathbf{x}_I$ of the nodal particles:

$$\mathbf{x} = N_I\mathbf{x}_I \tag{4.41}$$

where N are the interpolation(shape) functions and $\boldsymbol{\xi}$ represents the natural coordinates. For the same procedure, the displacement $\mathbf{u}$ and the gradient of it also can be interpolated as:

$$\mathbf{u} = N_I\mathbf{u}_I \tag{4.42}$$

$$\nabla_0\mathbf{u} = \mathbf{u}_I \otimes \nabla_0 N_I \tag{4.43}$$

For the interpolations of different qualities, the shape functions can be chosen the same or different, depending on the choices of the element types. In most situations the quantities are interpolated by the same shape function. In the Galerkin weighted method the weighting function is chosen to be the same as the shape function, i.e.:

$$\delta\mathbf{u} = N_I\delta\mathbf{u}_I \tag{4.44}$$

The linearized integral equation over the internal virtual work Eq. (4.36) can be discretized as follows. We recall Eq. (4.36), and start the discretization in one element:

$$D\delta W^e_{in} = \int_{\Omega^e_0} \delta\mathbf{E} : \boldsymbol{C}_e : D\mathbf{E}[\mathbf{u}]d\Omega^e_0 + \int_{\Omega^e_0} \mathbf{S} : [(\nabla_0\mathbf{u})^T \cdot \nabla_0\delta\mathbf{u}]d\Omega^e_0 \tag{4.45}$$

It is known that the Green strain tensor $\mathbf{E}$ is a function of $\mathbf{u}$. We have:

$$\delta\mathbf{E} = \delta\mathbf{u}_I \otimes \mathbf{B}_{0I}(\nabla_0 N, \mathbf{u}) \tag{4.46}$$

$$D\mathbf{E} = \mathbf{u}_J \otimes \mathbf{B}_{0J}(\nabla_0 N, \mathbf{u}) \tag{4.47}$$

where $\delta\mathbf{E}$ represents the values in the integration points of one element, and $\mathbf{B}_{0I}$ is called $\mathbf{B}$ matrix relating the strains with the displacements . After some tensor calculations and a transformation between tensor form and matrix form, the right-hand part of the first term of Eq. (4.45) is expressed in the matrix form ([7]) as :

$$[\delta\mathbf{u}_I]^T\mathbf{K}^e{}_{mat}[\mathbf{u}_I] \tag{4.48}$$

with:

$$\mathbf{K}^{emat}_{IJ} = \int_{\Omega^e_0} \mathbf{B}^T_{0I} : \mathbf{C}_e : \mathbf{B}_{0J}(\nabla_0 N)d\Omega^e_0 \tag{4.49}$$

This stiffness matrix is called the material tangent stiffness matrix of one element because this term is associated with the rate of stress and then depends on the material response.

Consider now the second term of Eq. (4.45) in one element. We have:

$$\nabla_0 \delta\mathbf{u} = \delta\mathbf{u}_I \otimes \nabla_0 N_I \tag{4.50}$$

$$\nabla_0 \mathbf{u} = \mathbf{u}_J \otimes \nabla_0 N_J \tag{4.51}$$

Here we take the same shape function for interpolating $\mathbf{u}$ and $\delta\mathbf{u}$ in this case. Then:

$$\int_{\Omega_0^e} \mathbf{S} : [(\nabla_0 \mathbf{u})^T \cdot \nabla_0 \delta\mathbf{u}] d\Omega_0^e = \int_{\Omega_0^e} \mathbf{S} : [(\delta\mathbf{u}_I \cdot \mathbf{u}_J)\nabla_0 N \otimes \nabla_0 N] d\Omega_0^e \tag{4.52}$$

Eq. (4.52) is rewritten as:

$$(\delta\mathbf{u}_I \cdot \mathbf{u}_J) \int_{\Omega_0^e} [\nabla_0 N_I \cdot \mathbf{S} \cdot \nabla_0 N_J] d\Omega_0^e \tag{4.53}$$

Because the integral part is observed as the scalar and $\delta\mathbf{u} \cdot \mathbf{u} = \delta\mathbf{u} \cdot \mathbf{I} \cdot \mathbf{u}$ with the unit tensor $\mathbf{I}$, the second term can also be worked out in matrix form $\delta\mathbf{u} \cdot \mathbf{K}^e{}_{geo} \cdot \mathbf{u}$ with ([7]):

$$\mathbf{K}^e{}_{geoIJ} = \int_{\Omega_0^e} [\nabla_0 N_I \cdot \mathbf{S} \nabla_0 N_J] \mathbf{I} d\Omega_0^e \tag{4.54}$$

This term includes the current state of the stress and also illustrates that the deformation affects the geometry. For this reason the matrix above is called geometric stiffness matrix. Concluding for the discrete directional derivative of the weak form in one element, which account for the internal and external virtual works,

$$D\delta W^e = -\delta\mathbf{u}_I^T \cdot (\mathbf{K}^e{}_{matIJ} + \mathbf{K}^e{}_{geoIJ}) \cdot \mathbf{u}_J + D\delta W_{ex}{}^e (= 0) \tag{4.55}$$

$$\mathbf{K}_{IJ}^e = \mathbf{K}^e{}_{matIJ} + \mathbf{K}^e{}_{geoIJ} \tag{4.56}$$

The discrete directional derivative of the weak form in the total domain can be obtained as:

$$D\delta W = \sum D\delta W^e = \sum \delta\mathbf{u}_I \cdot (\mathbf{K}^e{}_{matIJ} + \mathbf{K}^e{}_{geoIJ}) \cdot \mathbf{u}_J = \delta\mathbf{u}_I \cdot \mathbf{K}_{IJ} \cdot \mathbf{u}_J \tag{4.57}$$

Furthermore, the virtual work of the equilibrium equations can also be discretized in a way similar to that above:

$$\begin{aligned} \delta W^e &= \int_{\Omega_0^e} \delta\mathbf{E} : \mathbf{S} d\Omega_0^e - \int_{\Omega_0^e} \delta\mathbf{u} \cdot \mathbf{b}_0 d\Omega_0^e - \int_{\Gamma_0^e} \delta u \cdot \mathbf{t} d\Gamma_0^e \\ &= \int_{\Omega_0^e} \delta\mathbf{u}_I \otimes \mathbf{B}_0 : \mathbf{S} d\Omega_0^e - \int_{\Omega_0^e} N\delta\mathbf{u}_I \cdot \mathbf{b}_0 d\Omega_0^e - \int_{\Gamma_0^e} N\delta\mathbf{u}_I \cdot \mathbf{t} d\Gamma_0^e \end{aligned} \tag{4.58}$$

Rearranging this equation in matrix form:

$$\delta W^e = \delta \mathbf{u}_I^T \cdot (\int_{\Omega_0^e} \mathbf{B}_0{}^T \cdot \mathbf{S} d\Omega_0^e - \int_{\Omega_0^e} N\mathbf{f}_0 d\Omega_0^e - \int_{\Gamma_0^e} N\mathbf{t} d\Gamma_0^e) \tag{4.59}$$

In terms of the nodal internal force $\mathbf{T}_I^e$ and the external force $\mathbf{F}_I^e$ in one element, the equation above can be rewritten as:

$$\delta W^e = \delta \mathbf{u}_I \cdot (\mathbf{T}_I^e - \mathbf{F}_I^e) \tag{4.60}$$

where:

$$\mathbf{T}_I^e = \int_{\Omega_0} \mathbf{B}_0{}^T \cdot \mathbf{S} d\Omega_0 \tag{4.61}$$

$$\mathbf{F}_I^e = \int_{\Omega_0} N\mathbf{f}_0 d\Omega_0 + \int_{\Gamma_0} N\mathbf{t} d\Gamma_0 \tag{4.62}$$

Finally the virtual work in the finite element mesh is:

$$\delta W = \sum \delta W^e = \sum \delta \mathbf{u}_I \cdot (\mathbf{T}_I - \mathbf{F}_I) = \delta u_I \cdot \mathbf{R}_I \tag{4.63}$$

When the body is in the equilibrium state, the nodal residual forces become zero.

4.4 Iteration Procedure

Recalling Eq. (4.26), there is a Newton-Raphson equation:

$$\delta W + D\delta W = 0 \tag{4.64}$$

with the discretized form as:

$$\delta \mathbf{u}^T \cdot (\mathbf{K} \cdot \mathbf{u} + \mathbf{R}) = 0 \tag{4.65}$$

Therefore:

$$\mathbf{K} \cdot \mathbf{u} = -\mathbf{R} = \mathbf{F} - \mathbf{T} \tag{4.66}$$

$\mathbf{F}$ is the external force. The iterative procedure is as follows for each step:

1 Initialize $\mathbf{F} = \mathbf{F}_0$,$\mathbf{T} = 0$,$i = 0$, $\mathbf{u} = 0$ and set tolerance errors (Tor).

2 IF ($\|\mathbf{R}\|/\|\mathbf{F}\|$) > Tor,$i = i + 1$, ELSE GO TO 7.

3 Calculate $\mathbf{K}$, and solve $\mathbf{K}_i\mathbf{u} = -\mathbf{R}$.

4 Update $\mathbf{x} = \mathbf{x} + \mathbf{u}$.

5 Find other parameters (stresses, strains, deformation tensor).

6 Calculate $\mathbf{T}$ and $\mathbf{R}$, GO TO 2

7 END.

Bibliography

[1] Malveren, L., E.: Introduction to the mechanics of a continuous medium, Prentice-Hall, New York, 1969

[2] Zienkiewicz, O.,C.: The finite element method (Third edition), Mcgraw-Hill Book Company (UK) Limited, 1979

[3] Spiering, R.,M.,E.,J., Grootenboer, H.J.: Eindige elementen methode in de *werktuigbouwkunde*, Dictaat Unversity of Twente, The Netherlands, 1993 (in Dutch)

[4] Jongschaap, R.,J.,J.: Toegepaste tensorrekening, Dictaat Unversity of Twente, The Netherlands (in Dutch)

[5] Huétink, J.: Plasticiteit en kruip, Dictaat Unversity of Twente, The Netherlands, 1994 (in Dutch)

[6] Mooi, H.: Finite element simulations of aluminium extrusion, PhD thesis Unversity of Twente, The Netherlands, 1996

[7] Bonet, J., Wood, R.D.: Nonlinear continuum mechanics for finite element analysis, Cambridge University Press, 1997

[8] Belytschko, T., Liu, W.K., Moran, B.: Nonlinear finite elements for continua and structures. John Wiley and Sons Ltd., England, 2001

Chapter 5

Displacement Based Steady State Formulation

Go for details

Our project is concentrated on the simulation of steady state flow processes. In [1] coupled FE calculations with the material evolution equations in a referential configuration are used. However, this requires a complicated coordinate system transformation. In this chapter, a displacement based steady state formulation is constructed based on the ideas from [1].

Two basic expressions are involved in this steady state formulation: the material evolution equations and the equilibrium equations. These can be solved as a coupled or an uncoupled set using FEM. Only the uncoupled approach is examined here. The equilibrium equations are expressed in the undeformed configuration. The material evolution equations in our case ([3]) are different from the usual steady state solution methods (See *Chapter* 3). These equations are not expressed by the velocity $\boldsymbol{v}$ of a particle with material coordinates $\mathbf{X}$ in Eulerian description, but by the initial velocity $\boldsymbol{v}_0$. In Balagangadhar's method, the material evolution equations are expressed by the velocity in the referential configuration $\boldsymbol{v}_r$.

In the first section the governing equations for the steady state formulation are discussed. The stabilized FEM must be taken into account for reducing numerical oscillation problems, when solving the differential equations. In the second part this issue is considered; furthermore, a calculation procedure is proposed in the third section. Finally, since a forming process involves the interaction of two or more bodies, the contact problem is an important issue. In order to apply this steady state formulation to the real industrial processes, the contact problem cannot be ignored. In our case, since the solution procedure is different from other classical methods for steady state flow problems, the contact analysis becomes unique for the de-

veloped steady state formulation. This discussion is discussed in Section 5.4.

5.1 Governing Equations

In the steady flow calculations the governing equations include the equilibrium equations, the constitution relations, boundary conditions and material evolution (convection) equations.

5.1.1 Equilibrium

The equilibrium equations are Eq.(2.40):

$$\nabla \cdot (\mathbf{FS}) + \mathbf{b}_0 = 0 \tag{5.1}$$

With boundary conditions:

$$\mathbf{u} = \mathbf{u}_0 \quad \text{on } \Gamma_{u0} \tag{5.2}$$

$$\boldsymbol{S} \cdot \mathbf{n}_0 = \mathbf{t}_0 \quad \text{on } \Gamma_{t0} \tag{5.3}$$

where $\mathbf{n}_0$ is the outward normal with respect to the boundary, $\mathbf{t}_0$ represents the surface traction on surface Γ_{t0} and $\mathbf{u}_0$ is the prescribed displacement on surface Γ_{u0}.

5.1.2 Constitutive Relations

The constitutive relations depend on the material models that are chosen. In our case, hyperelastic-plastic constitutive models are chosen, and the stresses can be described as the function of Lagarangian strains:

$$\mathbf{S} = f(\mathbf{E}^e) \tag{5.4}$$

where $\mathbf{E}^e$ represents the elastic strain.

The yield function is written as:

$$\phi(\mathbf{S}, \mathbf{q}) = 0 \tag{5.5}$$

where $\mathbf{q}$ is a set of internal variables which is governed by the hardening or softening law of metal deformation.

The flow rule is specified as (see Eq. (2.84)):

$$\dot{\mathbf{E}}^p = \mathbf{Y} : \dot{\mathbf{E}} \tag{5.6}$$

where $\mathbf{Y}$ is a four order tensor, which can be obtained from the consistency condition and the yield function.

5.1.3 Convection Equations

In order to obtain the plastic strain further in the steady state problem, the convection equations must to be considered. The convection equations in Eulerian description:

$$\boldsymbol{v} \cdot \nabla \mathbf{E}^p = \dot{\mathbf{E}}^p \tag{5.7}$$

A detailed description of the convection equations in our steady state formulation can be found in the following section.

5.2 Material Evolution Equations

5.2.1 Developed Material Evolution Equations

The material evolution equations are derived from the expression of the material derivative of an arbitrary state variable in Eulerian way. The expression is repeated for steady state:

$$\dot{f} = \boldsymbol{v} \cdot \nabla f \tag{5.8}$$

We then transform this convection form from the deformed configuration to the undeformed configuration for the steady state:

$$\boxed{\dot{f} = \boldsymbol{v} \cdot \nabla f = (\boldsymbol{v}_0 \cdot \mathbf{F}^T) \cdot (\mathbf{F}^{-T} \cdot \nabla_{\mathbf{0}} f) = \boldsymbol{v}_0 \cdot \nabla_{\mathbf{0}} f} \tag{5.9}$$

where $\nabla_{\mathbf{0}}$ is the gradient in the undeformed configuration. In this form the coordinate system transformation is not required as in the method of Balagangadhar (see *Chapter* 3). The analysis is steady and the material state variables can be obtained via integration along the known path-line in the undeformed configuration. The characteristics of this form are described in Figure 5.1. The solid line block and grey block represent the initial and

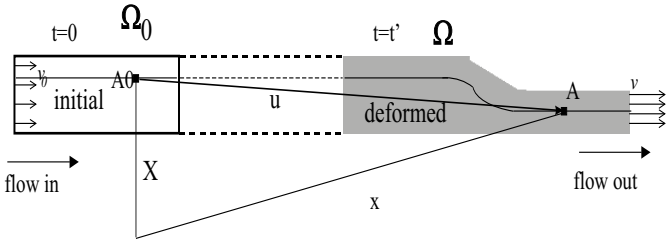

Figure 5.1: New description of steady flow processes

deformed situations, respectively. The blocks are connected using two dotted lines. These two lines indicate the flow pattern between time t_0 (initial time)

and time t (certain process time). The characters A_0 and A stand for any material particle in the initial mesh and deformed mesh, respectively. Each material particle A in the deformed situation corresponds to a particle A_0 in the initial situation during the steady flow process.

5.2.2 Stabilized FEM for Convection

The convection-diffusion equation system can be written as:

$$\frac{\partial f}{\partial t} + \boldsymbol{v} \cdot \nabla f + \nabla \cdot \mathbf{K} \nabla f = g \tag{5.10}$$

where g is the source vector. The second term in the above equation is the convection term and the third term is the diffusion term.

An important parameter indicating the character of the flow is the element *Péclet* number which is defined as:

$$P\acute{e} = \frac{vL}{\kappa} \tag{5.11}$$

where L is the length scale and κ is the diffusion coefficient. If $P\acute{e} \gg 1$ convection dominates the solution of the convection-diffusion problem, the results show an abrupt change within very few elements and the numerical oscillations occur using the Galerkin method ([4],[5]). The oscillations become worse for a larger *Péclet* number.

The material evolution expression as in Eq.(5.9) is the convection equation with a convection term only. The *Péclet* number is equal to infinity. Clearly, if the Galerkin formulation is applied for solving these equations, numerical oscillations cannot be avoided. For this reason stabilized methods have been developed for convection dominated equations.

Two stabilized methods are investigated here, the Streamline Upwind Petrov Galerkin functions (SUPG) and the Least Squares method (LS). SUPG, from a recent perspective, is one of the methods showing reasonable accuracy and stability properties. The Least Squares FE method has also been tested for the stability of the solutions in the convection equation. It is based on the minimization of the residuals in a least squares sense, and the theory and applications can be found in [4], [6] and [7]. When these kinds of methods are applied to finite element calculations, we call these methods "stabilized finite element methods".

The schematic descriptions of Galerkin, $SUPG$ and LS weighting functions are illustrated in Fig. 5.2.

For the Galerkin formulation, the convection equation Eq. (5.9) has the weak form as:

$$\int \delta f \cdot (\boldsymbol{v}_0 \cdot \nabla_{\mathbf{0}} f) dV = \int \delta f \cdot \dot{f} dV \tag{5.12}$$

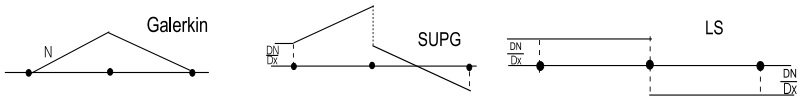

Figure 5.2: Three different weighting functions

For $SUPG$ and the LS method, the weak forms are expressed, respectively:

$$\int (\delta f + \gamma \boldsymbol{v}_0 \cdot \nabla_{\mathbf{0}} \delta f) \cdot (\boldsymbol{v}_0 \cdot \nabla_0 f) dV = \int (\delta f + \gamma \boldsymbol{v}_0 \cdot \nabla_{\mathbf{0}} \delta f) \cdot \dot{f} dV \tag{5.13}$$

and:

$$\int (\boldsymbol{v}_0 \cdot \nabla_{\mathbf{0}} \delta f) \cdot (\boldsymbol{v}_0 \cdot \nabla_0 f) dV = \int (\boldsymbol{v}_0 \cdot \nabla_{\mathbf{0}} \delta f) \cdot \dot{f} dV \tag{5.14}$$

where the parameter γ is the intrinsic time scale.

5.2.3 Tests with Three Weighting Methods

First, in order to compare the numerical results with the analytical solutions when solving Eq. (5.9), a one-dimensional test with 4-node elements is defined with nine integration points in one element. The material derivatives $\dot{f}$ are known at the integration points. A prescribed nodal value of f is given at the inflow boundary.

In Fig. 5.3 the material derivatives $\dot{f}$ are given as constants within one

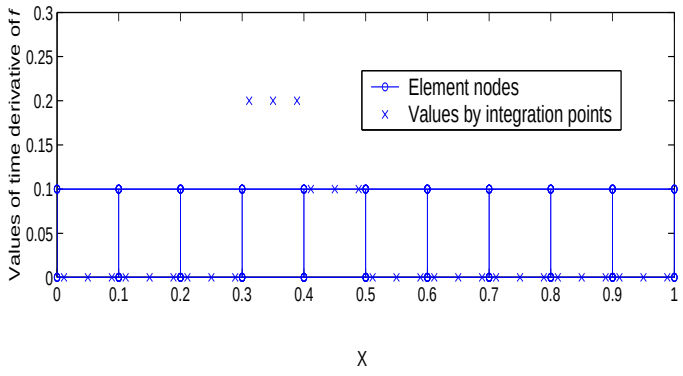

Figure 5.3: Case 1: Input and element mesh in 1D case

element by the integration points. The analytical solutions are compared to the numerical solutions obtained from Galerkin, $SUPG$ and LS method. The results are shown in Fig. 5.4. From this figure it is found that the results from these three weighting methods agree with those from analytical

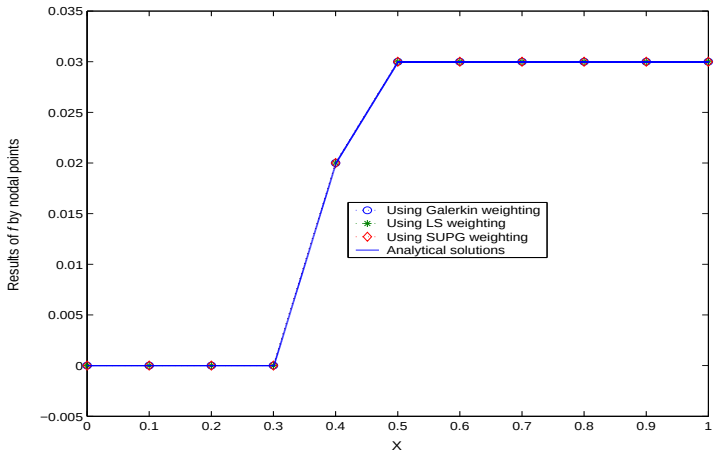

Figure 5.4: Case 1: Comparison between the analytical solutions and the results from three weighting functions

solutions No difference, however, cannot be seen between these three methods. The input values in this case within one element are constant, so that the nodal values in FEM are exact.

A further case was also checked with a non-constant input of the material time derivatives within one element. The mesh and input of the material time derivatives are shown in Fig. 5.5 and the results are shown in Fig. 5.6. It is apparent that the Galerkin method gives most spurious oscillation. Even though the $SUPG$ method gives better solutions than the Galerkin method , the LS method gives a more stable result than the $SUPG$ method.

The further applications of Galerkin, $SUPG$ and LS methods were

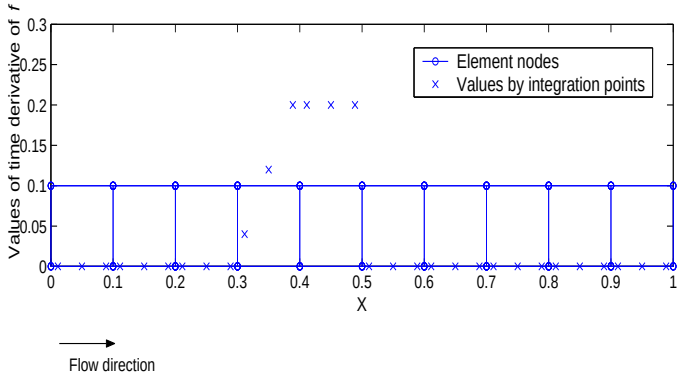

Figure 5.5: Case 2: Input and element mesh in 1D case

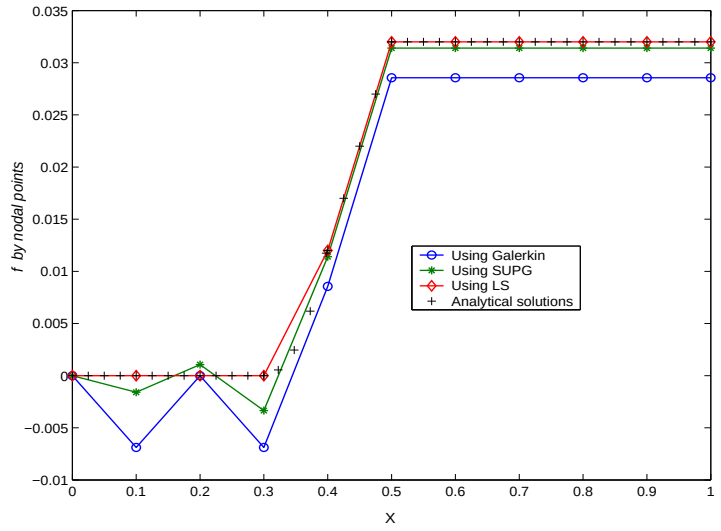

Figure 5.6: Comparison between the results from three weighting functions in 1D case

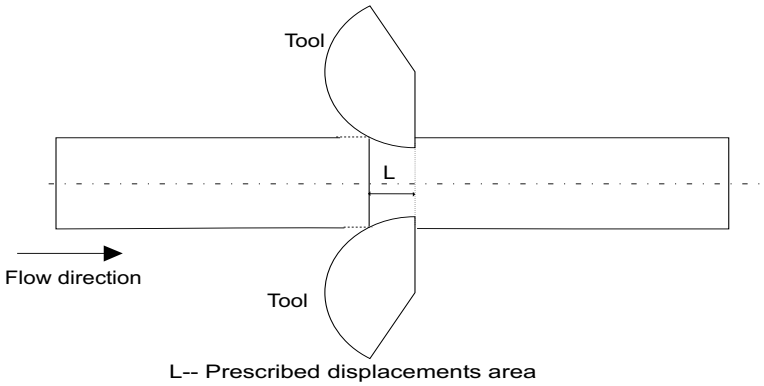

Figure 5.7: Set-up of the extrusion-like problem

implemented in a so-called extrusion-like problem with a purely elastic deformation. The set-up is shown in Fig. 5.7. Due to symmetry only half of the geometry needs to be modeled. The elastic deformed mesh can be found in Fig. 5.8.

The calculation procedure is described as follows:

Step 1 Initialize all the data. Set $\boldsymbol{S}_0 = 0$, $\mathbf{F} = \mathbf{I}$, $\mathbf{u} = 0$ etc.

Step 2 Process prescribed loads or displacements.

Step 3 Solve $[K] \cdot \Delta\mathbf{u} = F - R$ using FEM with pure elastic deformation

with stiffness matrix K. In case of nonlinearity an iterative method should be used. The iteration stops when the unbalance criterion is satisfied.

Step 4 With the help of the results for $\mathbf{u}$ calculate the strain $\mathbf{E} = \frac{1}{2}((\nabla_0 \mathbf{u})^T + \nabla_0 \mathbf{u} + \nabla_0 \mathbf{u} \cdot (\nabla_0 \mathbf{u})^T)$ directly.

Step 5 Calculate the flux of total strains $\dot{\mathbf{E}} = \mathbf{v}_0 \cdot \nabla_0 \mathbf{E}$.

Step 6 Calculate the strains using $\mathbf{v}_0 \nabla_0 \cdot \mathbf{E}^* = \dot{\mathbf{E}}$ from the flux of total strains .

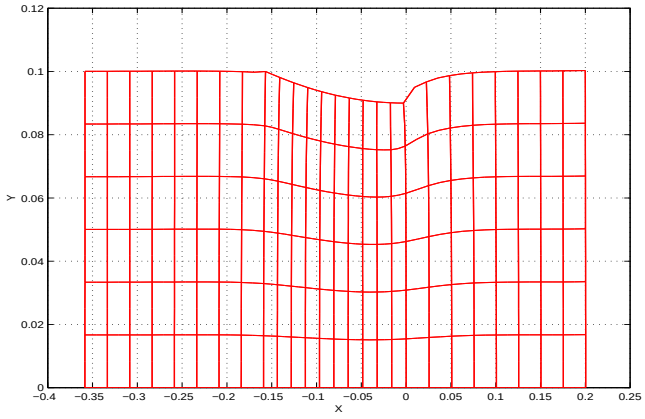

Figure 5.8: Deformed mesh with pure elastic deformation

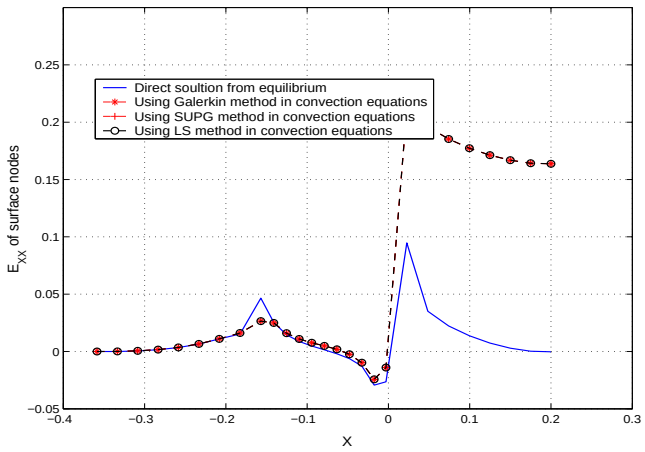

Figure 5.9: Results of E_{XX} with different weighting ways

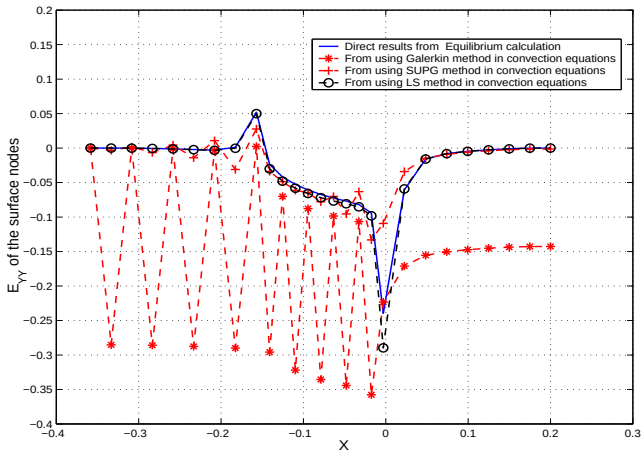

Figure 5.10: Results of E_{YY} with different weighting ways

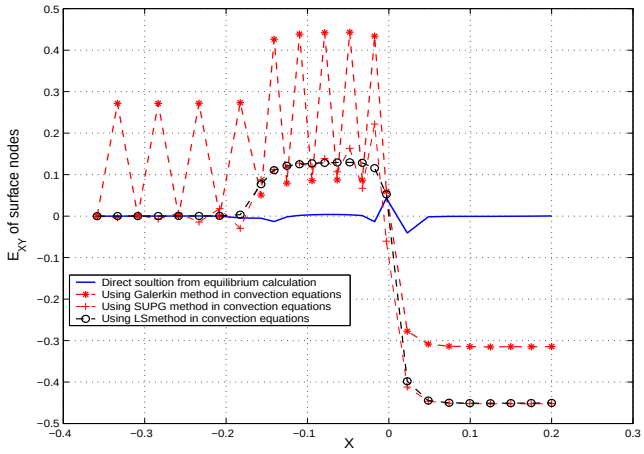

Figure 5.11: Results of E_{XY} with different choices of weighting

It is obvious that $\mathbf{E}^*$ must be equal to $\mathbf{E}$. The results obtained from using the different weighting functions in these convection equations, are shown in Fig. 5.9, Fig. 5.10 and Fig. 5.11. The same conclusions are drawn as for the previous case. Also here the superior stability of the Least Squares method is obvious. In fact, The Galerkin finite element method leads to oscillatory results. A similar behaviour is observed in the central difference method in the finite difference method. The *SUPG* uses upwinding strategies to represent the uni-directional character of the propagation phenomenon during the flow so that the numerical oscillations are reduced compared to the Galerkin method. However, the matrix of the resulting algebraic system is

nonsymmetric in $SUPG$. In [3] it is shown that the LS method has better control of the streamline derivative than the $SUPG$ and the matrix of the resulting algebraic system is symmetric and positive definite.

In our further research, in order to avoid the influence of the numerical oscillations when solving the convection equations, the LS method was chosen.

However even when using the LS method, the strains from the convection calculation $\mathbf{E}^*$ deviate from those obtained from direct calculation from the equilibrium equations $\mathbf{E}$. This is due to how the material time derivatives of $\mathbf{E}$ are calculated. The following section is therefore dedicated to this issue.

5.2.4 Material Time Derivatives of E

The material time derivatives of strains can be expressed as a convection equation ($\dot{\mathbf{E}} = \boldsymbol{v}_0 \cdot \nabla_0 \mathbf{E}$). There are two ways to calculate $\nabla_0 \mathbf{E}$:

- *Method 1*: Directly from displacements, which means that the second order derivatives of displacements are needed. The interpolation functions for the displacements are quadratic, and C_0 continuous across the element boundaries. Then, the strains are C_{-1} continuous. This means that the gradient of the strains does not exist at the element boundaries. This method was used in the previous section.
- *Method 2*: First obtain the nodal averaged strains $\mathbf{E}^n$ from the element strains and then use $\dot{\mathbf{E}} = \mathbf{v}_0 \cdot \nabla_0 \mathbf{E}^n$. The field of $\mathbf{E}^n$ is now continuous across the element boundary.

To check these two proposed methods we apply them again to the trivial problem, in which the material only deforms elastically (see Fig. 5.7 and Fig. 5.8). In this case the stresses are independent of the deformation history and hence can also be obtained in one step. They are both direct and indirect ways to calculate strains in pure elastic deformation:

- **Direct**: From the relation between the displacements and the strains.
- **Indirect**: From integration of the flux of the strains, which can be obtained by both *Method 1* and *Method 2* above.

Comparisons of strains obtained from both *Direct* and *Indirect* methods are shown in figs. 5.12, 5.13 and 5.14 for the strain components $\mathbf{E}_{XX}$, $\mathbf{E}_{YY}$ and $\mathbf{E}_{XY}$. In the *Indirect* method, both *Method 1* and *Method 2* are used, respectively. It is clearly seen that *Method 2* gives better results than *Method 1* for calculating $\mathbf{E}_{XX}$ and $\mathbf{E}_{XY}$. *Method 1* is better for $\mathbf{E}_{YY}$, but there is only local deviation in *Method 2*. For this reason, *Method 2* was chosen for further applications.

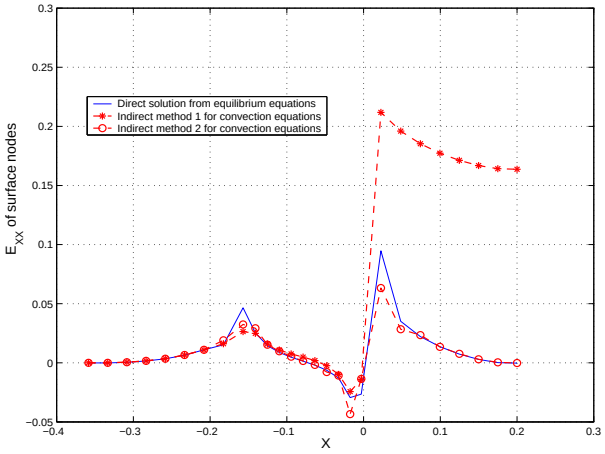

Figure 5.12: E_{XX} of surface nodes along along the direction of flow

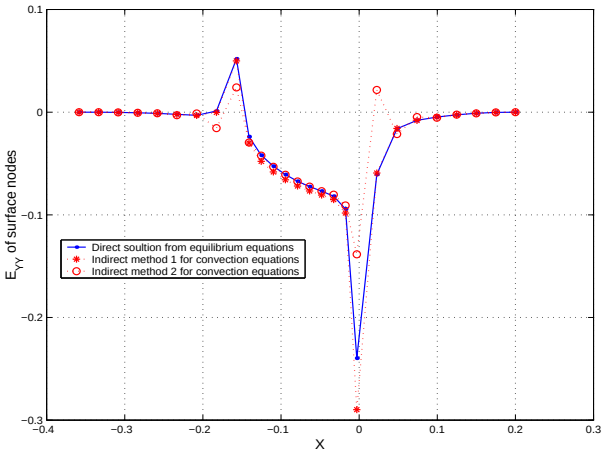

Figure 5.13: E_{YY} of surface nodes along the direction of flow

5.3 Solution Algorithm

The calculation procedure for an elastic plastic model based on the developed evolution equations is as follows:

Step 1 Initialize all the data. Set $\boldsymbol{S}_0 = 0$, $\mathbf{F} = \mathbf{I}$, $\mathbf{u} = 0$ etc.

Step 2 Process prescribed loads or displacements.

Step 3 Solve $[K]\cdot\Delta\mathbf{u} = F - R$ using FEM with pure elastic deformation with a stiffness matrix K. In the case of nonlinearity an iterative method

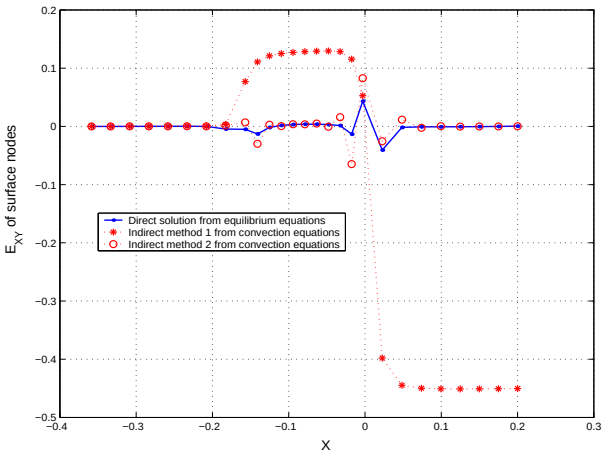

Figure 5.14: E_{XY} of surface nodes along the direction of flow

should be used. The iteration stops when the unbalance criterion is satisfied.

Step 4 Calculate the strains $\mathbf{E} = \frac{1}{2}((\nabla_0 \mathbf{u})^T + \nabla_0 \mathbf{u} + \nabla_0 \mathbf{u} \cdot (\nabla_0 \mathbf{u})^T)$.

Step 5 Calculate the flux of total strains $\dot{\mathbf{E}} = \boldsymbol{v}_0 \cdot \nabla_0 \mathbf{E}$.

Step 6 Obtain the time derivative of the plastic strains $\dot{\mathbf{E}}^p = \mathbf{Y} \cdot \dot{\mathbf{E}}$.

Step 7 Obtain the plastic strains with the developed evolution equations $\boldsymbol{v}_0 \cdot \nabla_0 \mathbf{E}^p = \dot{\mathbf{E}}^p$

Step 8 Calculate the total stresses from Eq. (5.4). Because tensor $\mathbf{Y}$ depends on the total stresses, an iterative method should be used until a convergence criterion is satisfied. The iterative steps begin from Step 6.

Step 9 Solve:

$$[K] \cdot \Delta \mathbf{u} = F - R$$

where R represents the element reaction forces. Iterative steps should be taken as from Step 3.

It can be observed that this computation procedure does not require the transient solution of the process. First the elastic calculation should be carried out so that the displacements are obtained to calculate the fluxes of the total strains and the fluxes of the plastic strains. Once these results are known, the nodal plastic strains can be calculated from the integration of the fluxes of the plastic strains. Afterwards, the discontinuous stresses are

calculated. Plastic deformation takes place in the loading region. Elastic spring-back is expected in the unloading part.

5.4 Contact Analysis

When the points on a boundary of one body contact with points on the boundary of the same or another bodies, the contact problems will be considered. In many industrial processes, the contact problems cannot be ignored due to the contact forces generated during processing. In order to find an appropriate manner for describing the contact for our case, the analysis based on [8] and [9] is studied for general problems, such as impact problems or flow problems with transient calculations.

The sum of the internal virtual work and the virtual work of applied forces and traction for the bodies should balance the virtual work of the contact forces acting on contact bodies Γ^i:

$$\begin{aligned} G^i(\boldsymbol{\varphi}^i, \delta\mathbf{u}^i) = \int_{\Omega_0^i} \mathbf{S} : \delta\mathbf{E}^i d\Omega_0^i - \int_{\Omega_0^i} \mathbf{b}^i : \delta\mathbf{u}^i d\Omega_0^i - \int_{\Gamma_{s0}^i} \mathbf{t} : \delta\mathbf{u}^i d\Gamma^i{}_{s0} \\ = \int_{\Gamma_{c0}^i} \mathbf{t}_c : \delta\mathbf{u}^i d\Gamma_{c0}^i \end{aligned} \tag{5.15}$$

This equation must hold for each body (i) and for all time t. The quantity $G^i(\boldsymbol{\varphi}^i, \delta\mathbf{u}^i)$ is the sum of the internal virtual work and the virtual work of the applied forces and traction for body i. Briefly([8],[9]):

$$G^i(\boldsymbol{\varphi}^i, \delta\mathbf{u}^i) + G_c^i(\boldsymbol{\varphi}^i, \delta\mathbf{u}^i) = 0 \tag{5.16}$$

with:

$$G_c^i(\boldsymbol{\varphi}^i, \delta\mathbf{u}^i) = -\int_{\Gamma_c^i} \mathbf{t}_c^i \cdot \delta\mathbf{u}^i \, d\Gamma^i \tag{5.17}$$

The contact force induced on body 2 is equal and opposite to that induced on body 1 at the contact area, i.e.

$$\mathbf{t}_c^2 = -\mathbf{t}_c^1 \tag{5.18}$$

Therefore:

$$G_c^i(\boldsymbol{\varphi}^i, \delta\mathbf{u}^i) = -\int_{\Gamma_c^1} \mathbf{t}_c^1 \cdot (\delta\mathbf{u}^1 - \delta\mathbf{u}^2) \, d\Gamma_c^1 \tag{5.19}$$

Resolving the contact forces and the virtual displacements into normal and tangential components gives the following statement of the contact virtual work ([1]):

$$G(\boldsymbol{\varphi}, \delta\mathbf{u}) = \int_{\Gamma^1} [t_{cn}^1 \cdot \delta dN + t_{ct}^1 \cdot \delta dt] \, d\Gamma^1 \tag{5.20}$$

where dN is the distance from body 1 to body 2 (see Fig. 5.15) and dt is the tangential shift. If using a penalty method, the contact traction can be described as:

$$t_{cn} = PdN \tag{5.21}$$

provided:

$$dN \leq 0 \tag{5.22}$$

P is the penalty number. In the Coulomb friction model, calculation of the tangential force follows the following conditions with both slip and stick states:

$$\phi = t_{ct} - \mu t_{cn} < 0 \qquad \text{stick} \tag{5.23}$$

$$t_{ct} = P_t dt \qquad \text{stick} \tag{5.24}$$

$$t_{ct} = \mu t_{cn} \qquad \text{slip} \tag{5.25}$$

P_t is the penalty number for tangential traction and dt is the the slip distance.

As described earlier, the contact algorithm is split into two parts: normal and tangential contact traction. The virtual work in the normal direction can be described as:

$$\begin{aligned} G_{cn} &= [\delta \mathbf{u}] \cdot \int_\Gamma PdN \cdot \delta dN \, d\Gamma \\ &= \int_\Gamma PdN \cdot \nabla_{\mathbf{u}} dN \, d\Gamma \end{aligned} \tag{5.26}$$

From this equation, the normal reaction forces can be worked out:

$$\mathbf{R}_{cn} = \int_\Gamma PdN \cdot \nabla_{\mathbf{u}} dN \, d\Gamma \tag{5.27}$$

The stiffness $\mathbf{K}_{cn}$ will be:

$$\mathbf{K}_{cn} = \int_\Gamma (P(\nabla_{\mathbf{u}} dN) + PdN(\nabla_{\mathbf{u}} \nabla_{\mathbf{u}} dN)) \, d\Gamma \tag{5.28}$$

The closest distance between the two bodies should be sought during the simulation as described in Figure 5.15; i.e. the distance between a surface point **a** (nodal point or integration point) on surface of body 1 and the surface elements of body 2 should be calculated one by one to find which element is closest to point **a**. The details of how to determine dN, $\nabla_{\mathbf{u}} dN$ and $\nabla_{\mathbf{u}} \nabla_{\mathbf{u}} dN$ can be found in Appendix C.

For slip, the virtual contact work in the tangential direction is written as:

$$R_{ct} = \int_\Gamma (P\mu dN \nabla_{\mathbf{u}} dt) \, d\Gamma \tag{5.29}$$

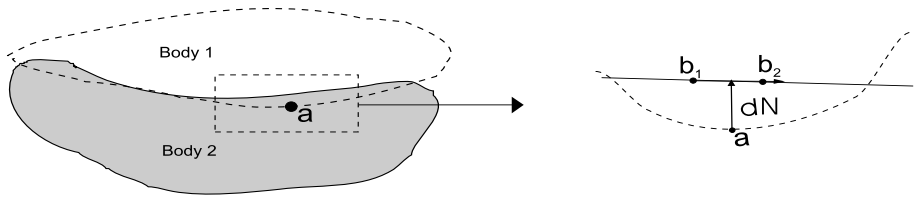

Figure 5.15: Schematic depicting gap definition between two contacting bodies

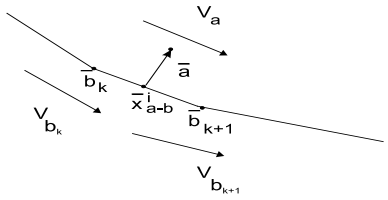

Figure 5.16: Description of slip in our steady state problem

Therefore, the stiffness $\mathbf{K}_{ct}$ is expressed as:

$$\mathbf{K}_{ct} = \int_{\Gamma} \nabla_{\mathbf{u}} dt^T P \mu \nabla_{\mathbf{u}} dN \, d\Gamma + \int P \mu dN \nabla_{\mathbf{u}} \nabla_{\mathbf{u}} dt^T \, d\Gamma \tag{5.30}$$

In impact problems or transient calculations, the slip theory concerning the relative movement between two calculation steps is used (see Appendix D). However, if the steady state calculations are carried out, the slip for steady state calculations should be defined as the relative movement between the bodies (See Fig 5.16). One conclusion is that the slip theory in the contact method used in most impact problems or transient calculations could not be used directly for our steady state case. However, the theory to obtain the normal tensor can still be applied for our formulation.

5.4.1 A Contact Method

In our case, assuming that the tool is considered to be rigid, the weak form is:

$$G(\mathbf{u}, \delta\mathbf{u}) = \int_{\Gamma^{(1)}} \mathbf{t}_c^1 \cdot \delta\mathbf{u}^1 \, d\Gamma^1 \tag{5.31}$$

with:

$$\mathbf{t}_c^1 = \begin{bmatrix} t_{cx} \\ t_{cy} \end{bmatrix} \tag{5.32}$$

The contact forces can be split into the normal and tangential directions to the surface:

$$\mathbf{t}_c'^1 = \begin{bmatrix} t_{ct} \\ t_{cn} \end{bmatrix} \tag{5.33}$$

The values should be transformed from the local to the referenced configuration.

The reaction force is given by:

$$\mathbf{R}_c = \int_\Gamma \mathbf{Q} \cdot \mathbf{t}_c'^1 \, d\Gamma^1 \tag{5.34}$$

where $\mathbf{Q}$ is the transformation tensor. As well known:

$$t_{cx} = t_{ct}\mathbf{t}_t \cdot \mathbf{e}_x + t_{cn}\mathbf{n} \cdot \mathbf{e}_x \tag{5.35}$$

$$t_{cy} = t_t\mathbf{t}_{ct} \cdot \mathbf{e}_y + t_{cn}\mathbf{n} \cdot \mathbf{e}_y \tag{5.36}$$

therefore:

$$\mathbf{t}_c = (\mathbf{t}_t \otimes \mathbf{e}_x + \mathbf{n} \otimes \mathbf{e}_y) \cdot \mathbf{t}'_c \tag{5.37}$$

with:

$$\mathbf{Q} = \mathbf{t}_t \otimes \mathbf{e}_x + \mathbf{n} \otimes \mathbf{e}_y \tag{5.38}$$

$\mathbf{t}_t$ and $\mathbf{n}$ are the unit tensors with relation to the angle between the normal tensor and the reference configuration and can be obtained by the calculation of the shortest distance between two bodies.

Hence, the stiffness will be:

$$K_c = \int_\Gamma (\mathbf{Q} \cdot \nabla_\mathbf{u}\mathbf{t}'_c + \nabla_\mathbf{u}\mathbf{Q} \cdot \mathbf{t}'_c) \, d\Gamma^1 \tag{5.39}$$

with:

$$\nabla_\mathbf{u}\mathbf{Q} = \nabla_\mathbf{u}\mathbf{t}_t \otimes \mathbf{e}_x + \nabla_\mathbf{u}\mathbf{n} \otimes \mathbf{e}_y \tag{5.40}$$

Due to:

$$(\mathbf{S} \otimes \mathbf{v}) \cdot \mathbf{u} = (\mathbf{u} \cdot \mathbf{v})\mathbf{S} \tag{5.41}$$

therefore:

$$\nabla_\mathbf{u}\mathbf{Q} \cdot \mathbf{t}'_c = (\nabla_\mathbf{u}\mathbf{t}_t \otimes \mathbf{e}_x + \nabla_\mathbf{u}\mathbf{n} \otimes \mathbf{e}_y) \cdot \mathbf{t}'_c = (\mathbf{e}_x \cdot \mathbf{t}'_c)\nabla_\mathbf{u}\mathbf{t}_t + (\mathbf{e}_y \cdot \mathbf{t}'_c)\nabla_\mathbf{u}\mathbf{n} \tag{5.42}$$

This contact algorithm was chosen for further applications, as shown in the following chapter.

Bibliography

[1] Balagangadhar, D., Tortorelli, D.A.: Design of large-deformation steady elastoplastic manufacturing processes. Part I: A displacement-based reference frame formulation. International Journal for Numerical Methods in Engineering. Vol. 49, 2000, 899-932

[2] Balagangadhar, D., Dorai, G.A., Tortorelli, D.A.: A displacement-based reference frame formulation for steady-state thermo-elasto-plastic material processes. International Journal of Solids Structures. Vol. 36, 1999, 2397-2416

[4] Yu, Y., Geijselaers, H.J.M., Huétink, J.: A new displacement based FE formulation for steady state problems, Simulation of Materials Processing: Theory, Methods and Applications, Mori (Eds), Proceedings of NUMIFORM'2001, Toyohashi, Japan, 2001, 121-126

[4] Jiang, B.: The least-squares finite element method, Theory and applications in computational fluid dynamics and electromagnetics, Springer-verlag Berlin Heidelberg New York, 1998, 1-30, 201-213

[5] Mooi, H.: Finite element simulations of aluminium extrusion, phD thesis University of Twente, Enschede, The Netherlands, 1996

[6] Jiang, B.: On the least-squares method, Computer Methods in Applied Mechanics and Engineering, Vol. 152, 1998, 239-257

[7] Moussaoui, F.: A unified approach for inviscid compressible and nearly incompressible flow by least-squares finite element method, Applied Numerical Mathematics, Vol. 44, 2003, 183-199

[8] Laursen, T.A., Simo, J.C.: A continuum-based finite element formulation for the implicit solution of multibody, large deformation frictional contact problem, International Journal for Numerical Methods in Engineering. Vol. 36, 1985, 3451-3485

[9] Simo, J., Lauren, T.A.: An augmented Lagrangian treatment of contact problems involving Friction, Computers Structures. Vol. 42, No.1, 1992, 97-116

[10] Wriggers, P., Vu Van, T., Stein, E.: Finite element formulation of large deformation impact-contact problems with friction, Computers and structures. Vol.37, No.3, 1990, 319-331

[11] Kloosterman, G., van Damme, R.M.J., van den Boogaard, A.H.: A geometrical-based contact algorithm using a barrier method, International Journal for Numerical Methods in Engineering. Vol.51, 2001, 865-882

[12] Belytschko, T., Liu, W.K., Moran, B.: Nonlinear finite elements for continua and structures. John Wiley and Sons Ltd., England, 2001

Chapter 6

Test Results

A step further

In Chapter 5 a developed steady state FE formulation is introduced theoretically and some related FEM problems are discussed. In this chapter we attempt to obtain the test results with two different material models: a linear material model and an nonlinear material model. The steady state formulation, which is outlined in preceding chapter, is implemented in several cases with two different material models. All the problems are plane strain problems. The simulations were all run using MATLAB. We used a quadrilateral element with 9 nodes to interpolate the displacement $\mathbf{u}$ and 4 nodes to interpolate the strain $\mathbf{E}$ and the plastic strain $\mathbf{E}^p$.

6.1 Linear Material Model

First, the finite element simulations were carried out with a linear material model which can be used for small strain deformations. In this material model the stress relates to the elastic strains linearly as:

$$\mathbf{S} = \mathbf{C}_{el} : \mathbf{E}^e = \mathbf{C}_{el} : (\mathbf{E} - \mathbf{E}^p) \tag{6.1}$$

This is called a Saint Venant-Kirchhoff material or a Kirchhoff material for brevity ([1]). $\mathbf{C}_{el}$ is the constant fourth order elastic moduli tensor. Many materials (such as metals) can be modelled as being isotropic for small strains. An isotropic tensor $\mathbf{C}_{el}$ was chosen for our calculation:

$$\mathbf{C}_{el} = \lambda \mathbf{I} \otimes \mathbf{I} + 2\mu \boldsymbol{I} \tag{6.2}$$

where the two independent material constants λ and μ are called the Lam*é* constants. $\boldsymbol{I}$ is the fourth order tensor with the components $\boldsymbol{I}_{ijkl} = \frac{1}{2}(\delta_{ik}\delta_{jl} + \delta_{il}\delta_{jk})$. The Lam*é* constants can be expressed in terms other constants, the

Young's modulus E and the Possion's ratio ν:

$$\mu = \frac{E}{2(1+\nu)}, \qquad \lambda = \frac{\nu E}{(1+\nu)(1-2\nu)} \tag{6.3}$$

The associative plastic theory in these calculations is treated as being similar to that in the hypoelastic-plastic model for linear isotropic hardening:

$$\phi(\mathbf{S}, q) = \|dev(\mathbf{S})\| - \sqrt{\frac{2}{3}}(S_{y0} + E_t \cdot q) \leq 0 \tag{6.4}$$

where $dev(\cdot)$ is the deviator of the tensor argument. S_{y0} is the initial yield stress, E_t is a constant with a positive value which represents the evolution of the isotropic hardening and q is the equivalent strain in this case. The evolution of $\dot{\mathbf{E}}^p$ is described as:

$$\dot{\mathbf{E}}^p = \dot{\lambda} dev(\mathbf{S}) \otimes dev(\mathbf{S}) : \dot{\mathbf{E}} \tag{6.5}$$

For pure elastic deformation and an unloading situation,

$$\dot{\lambda} = 0 \tag{6.6}$$

For plastic deformation:

$$\dot{\lambda} = \frac{1}{\|dev(\mathbf{S})\|^2(1 + \frac{E_t}{3\mu})} \tag{6.7}$$

Two steady state flow processes were modelled with this linear material model in the displacement-based formulation. One is a pure shear flow and second is a simple extrusion case.

6.1.1 Pure Shear Flow

The set-up of the pure shear test is shown in Fig. 6.1. The vertical arrows illustrate the prescribed displacement direction. The material flows in and then out through the loading region, and the load gives the material only pure shear deformation. Therefore the material by or after loading endure the pure shear deformation. The material will only retain the plastic deformation after flowing out of the loading region. The elastic spring-back should be observed at the flow-out part for an elastic-plastic material. The relation between shear stresses and shear strains is described as:

$$\tau_{xy} = \mu \gamma_{xy} \tag{6.8}$$

In this test the contact region is known in the undeformed configuration, and a contact analysis is therefore not required.

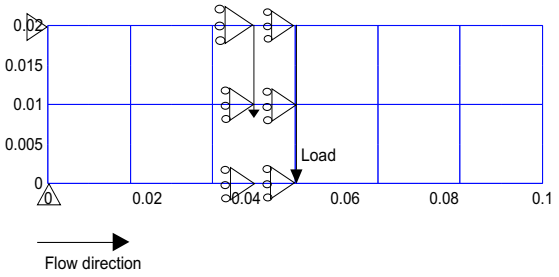

Figure 6.1: Set-up of pure shear flow

E	ν	E_t	S_{y0}	inflow velocity v_0
70Gpa	0.35	1Gpa	2Gpa	[1 0]

Table 6.1: The material parameters of the shear flow test

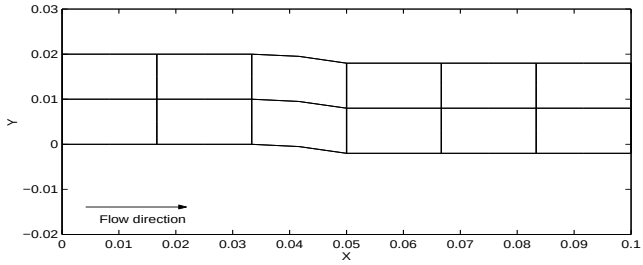

Figure 6.2: Pure elastic shear deformation

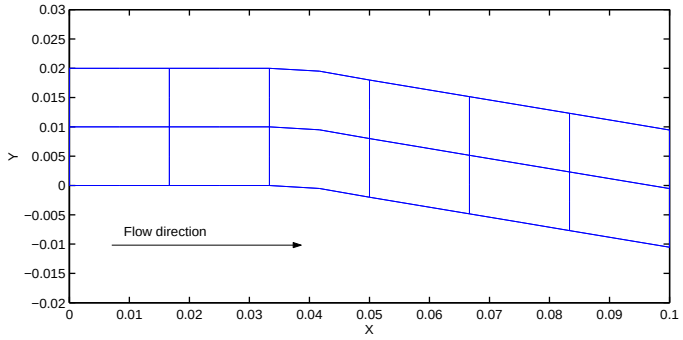

Figure 6.3: Elastic plastic deformation mesh

The parameters were chosen as given in Table 6.1. In order to see the spring-back more clearly, we chose the yield stress S_{y0} higher than that in practice.

In Fig. 6.2 the deformed mesh is shown when only a pure elastic defor-

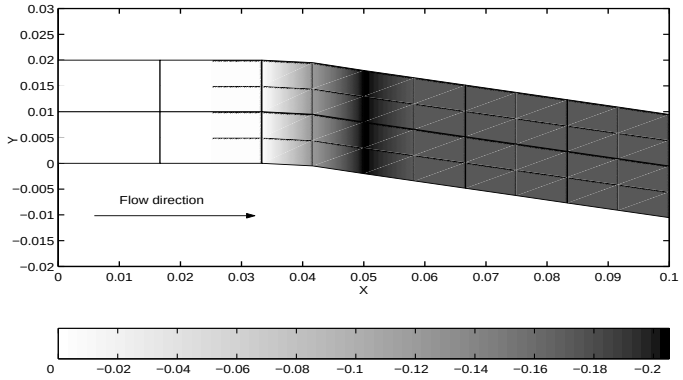

Figure 6.4: Total shear strains distribution

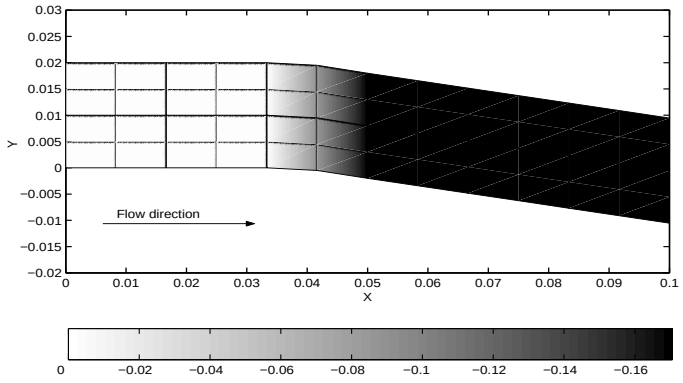

Figure 6.5: Plastic shear strains distribution

mation takes place in the simulation. It is found that the material recovers to the undeformed situation after unloading. In Fig. 6.3 the mesh with elastic plastic deformation is shown. The elements keep the plastic deformation after flowing out of the loading region. In order to observe the elastic spring-back in the simulation, the total shear strain distribution is shown in Fig. 6.4. It was found that the maximum shear strain is at the nodes which have the maximum prescribed displacements by the loading regions. In the flowing-out area the nodes have less total shear strains than those in the loading region, and that means that the material springs back elastically after unloading. The plastic shear strains reach a certain constant value after flowing out in Fig. 6.5.

The plastic strains and total strains along the streamline on the surface are shown in Fig. 6.6. In the loading area the plastic strains are smaller than the total strains due to elasticity. After the material flows out of the loading

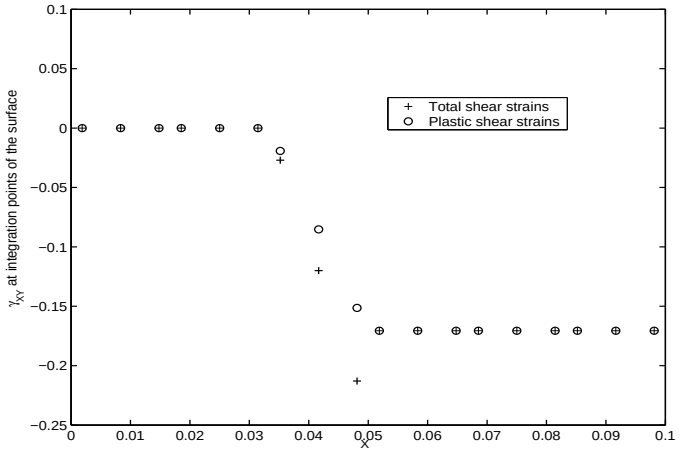

Figure 6.6: Total and plastic strains along streamline on surface

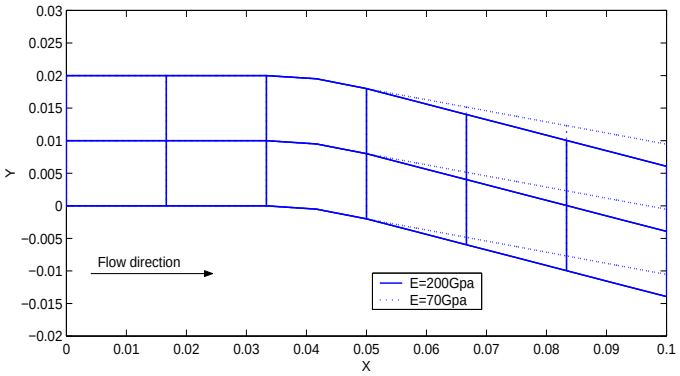

Figure 6.7: Elastic plastic deformed meshes with different elastic modulus

region, both strains overlap due to elastic spring-back after unloading. The elastic deformation becomes larger with decreasing elastic modulus, which can be seen in Fig. 6.7. With larger elastic deformation, the elements on the flow-out side spring back more.

6.1.2 Simple Extrusion Case

In this section a simple extrusion case is studied. Here, the contact region is unknown and a contact analysis must be carried out. Because the problem is axis-symmetric, only half of set-up is shown in Fig. 6.8. The material flows in, enters the tool and then flows out. The in-flow boundary is suppressed. The material properties were chosen as in Table 6.2.

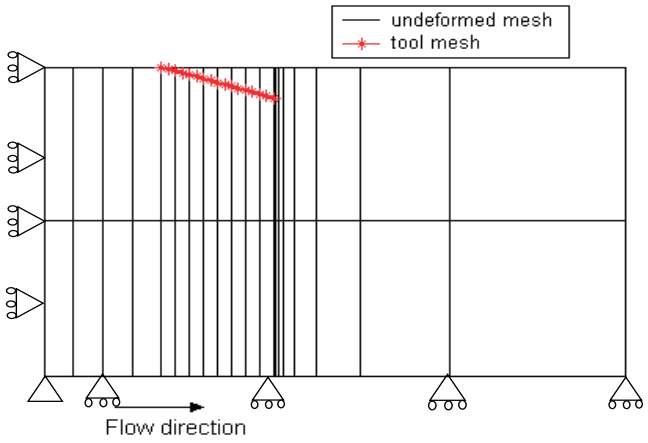

Figure 6.8: Undeformed mesh

The deformed mesh with the pure elastic deformation is shown in Fig. 6.9.

E	ν	E_t	S_{y0}	$[v_X, v_Y](m/s)$	Friction coefficient (μ)
70Gpa	0.35	1Gpa	2Gpa	[1 0]	0./0.2/0.4

Table 6.2: The material parameters of extrusion case in linear model

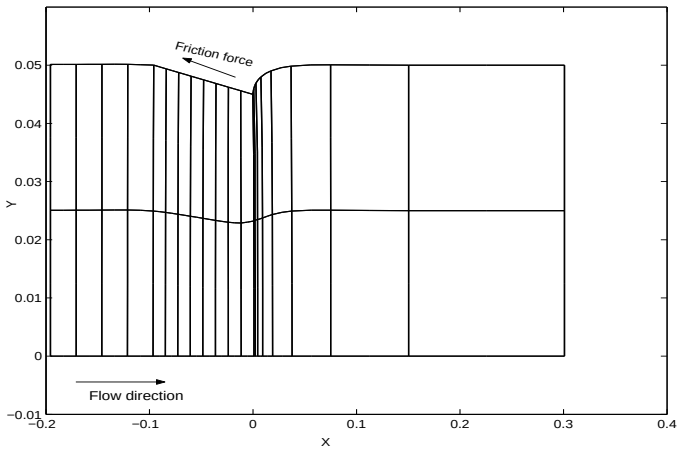

Figure 6.9: Pure elastic deformation mesh

In the extrusion process the friction between the tools and the specimen

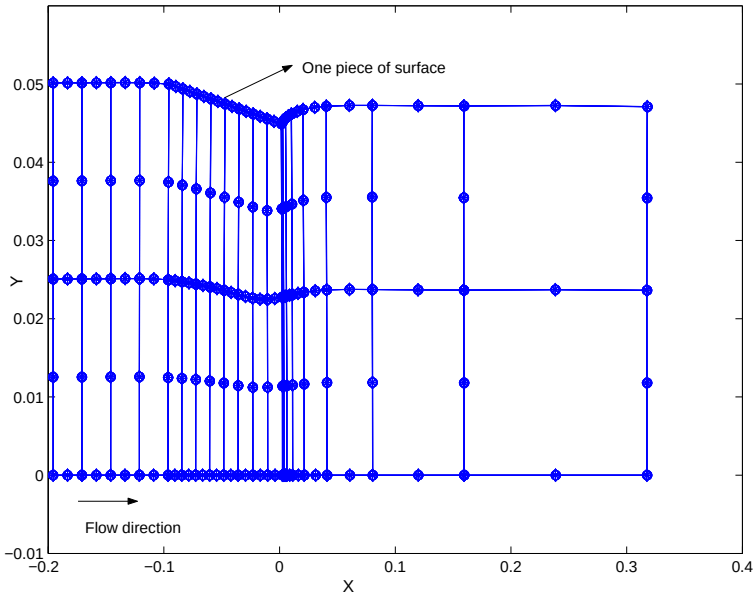

(a) Elastic-plastic deformed mesh with different friction coefficients

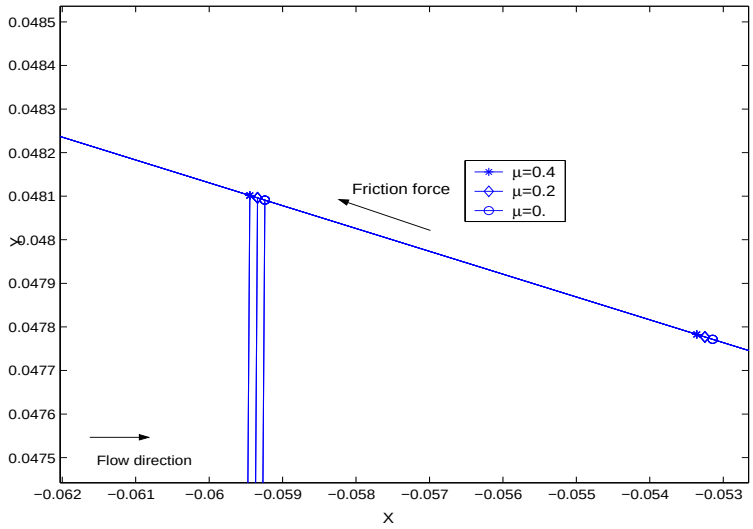

(b) Nodes on surface part with μ=0., μ=0.2, μ=0.4

Figure 6.10: Comparison of deformed mesh with three different friction coefficients

does not change direction. The contact algorithm described in the previous chapter was applied for this case. The results with different friction coefficients are shown in Fig. 6.10. With a larger friction the mesh flows more slowly.

The deformed mesh with the velocity plot is shown in Fig. 6.11 when the

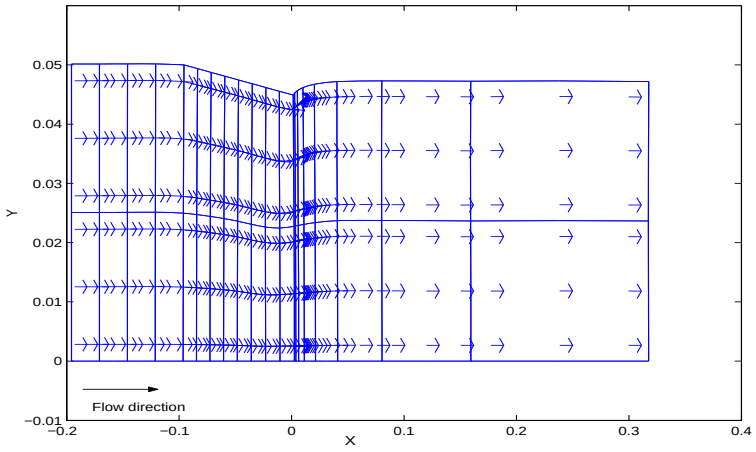

Figure 6.11: Deformed mesh with velocity vector plot

values of the initial velocities at the in-flow boundary are equal to $1.0m/s$. The velocities of the integration points were obtained from:

$$\boldsymbol{v} = \mathbf{F} \cdot \boldsymbol{v}_0 \tag{6.9}$$

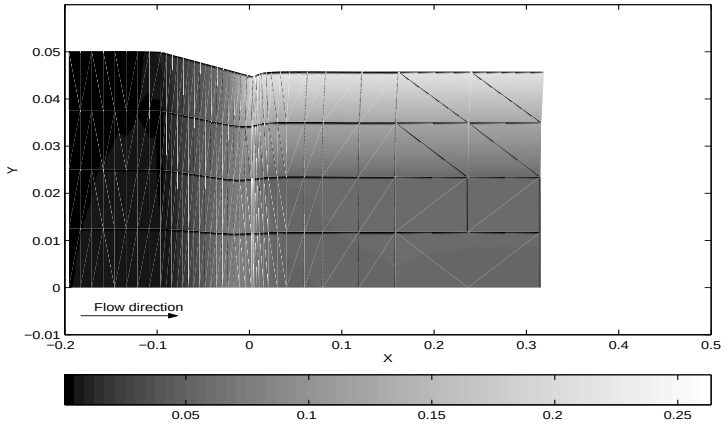

Figure 6.12: Equivalent total strain distribution

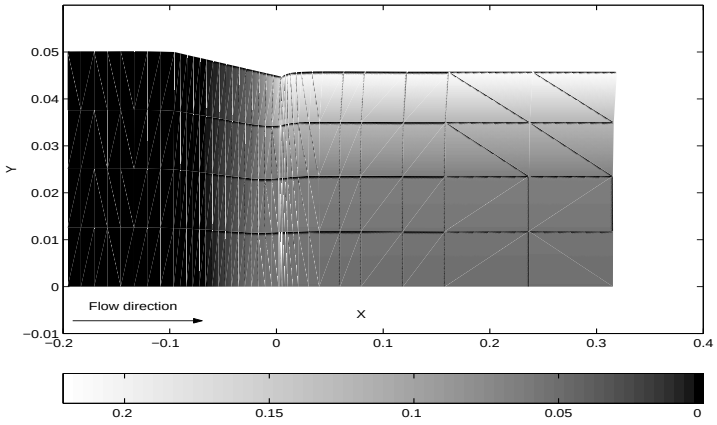

Figure 6.13: Equivalent plastic strain distribution

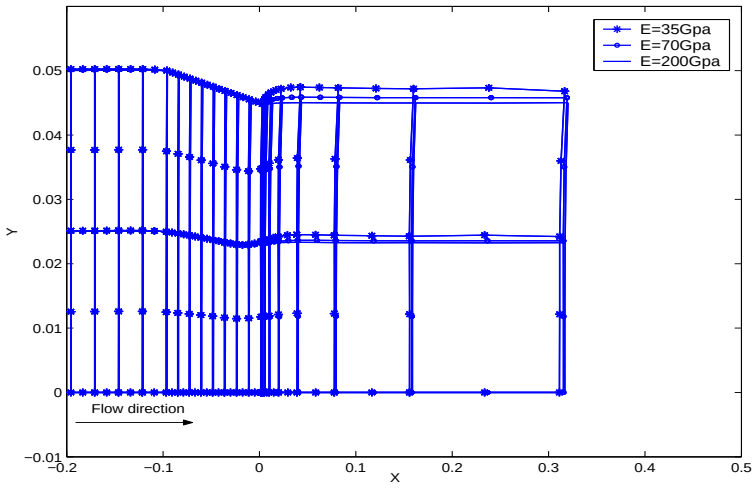

Figure 6.14: Deformed meshes with three different elastic moduli

The deformed mesh with equivalent strains distributions is shown in Fig. 6.12. The values at the largest loading area is larger than those in the flow-out region due to the elastic spring-back. Further, the deformed mesh with equivalent plastic strains is shown in Fig. 6.13. It is seen that the equivalent plastic strains reach the constant values from deformed area.

We know that the material properties play an important role in the deformation. For elasto-plastic materials the elastic deformation will be more when the specimen has a smaller elastic modulus. In our case the specimen

will spring back more after flowing-out with a smaller elastic modulus. In Fig. 6.14 three deformed meshes have different elastic spring-back when the deformation in these three cases is based on the different elastic moduli.

6.2 Nonlinear Material Model

In this section the hyperelastic plastic material model is applied. The introduction of this model was described in Chapter 2. In our case a stored-energy function was chosen of the form([2]):

$$\hat{\psi} = \frac{1}{2}\kappa[\frac{1}{2}(J^{e2} - 1) - lnJ^e] + \frac{1}{2}\mu(tr[\bar{b}^e] - 3) \tag{6.10}$$

where:

$$J^e := det[\mathbf{F}^e] \tag{6.11}$$

$$\bar{\mathbf{b}}^e := J^{e-2/3}\mathbf{F}^e \cdot \mathbf{F}^{eT} \tag{6.12}$$

κ and μ are interpreted as the bulk modulus and the shear modulus, respectively. The relations between these four material parameters κ, elastic modulus E and Possion's ratio ν is as follows:

$$\kappa = \frac{E}{3(1-2\nu)} \tag{6.13}$$

From this stored energy function the Second Piola-Kirchhoff stress has the form:

$$\mathbf{S} = \frac{1}{2}\kappa\mathbf{C}^{-1}(J^{e2} - 1) + \mu J^{e-\frac{2}{3}}DEV(\mathbf{C}^{p-1}) \tag{6.14}$$

in which DEV represents $DEV := (\cdot) - \frac{1}{3}[\mathbf{C} : (\cdot)]\mathbf{C}^{-1}$.
The Von Mises yield condition is used in the material description as ([2]):

$$\phi(\mathbf{S}, \mathbf{C}) = \sqrt{(\mathbf{C} \cdot \mathbf{S}) : (\mathbf{S} \cdot \mathbf{C}) - \frac{1}{3}(\mathbf{S} \cdot \mathbf{C})^2} - R \tag{6.15}$$

where R is the radius of the Von Mises sphere. The Kuhn-Tucker optimality condition then yields the associative flow rule:

$$-\mathbf{M} : \dot{\mathbf{E}}^p = \dot{\gamma}\frac{\partial\phi}{\partial\mathbf{E}} \tag{6.16}$$

where $\dot{\gamma}$ is the plastic consistency parameter, and $\mathbf{M}$ is defined as:

$$\mathbf{M}(\mathbf{E}, \mathbf{E}^p) = \frac{\partial\mathbf{S}}{\partial\mathbf{E}^p} \tag{6.17}$$

In order to test this model, a one-element test was carried out. Further, this model was applied to the same case as in section 6.1.1.

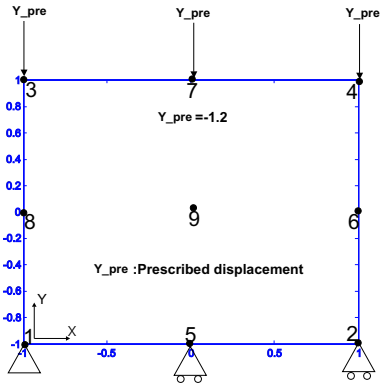

Figure 6.15: Set-up of one-element test

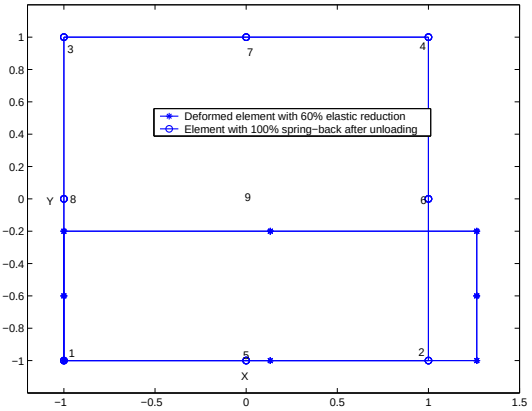

Figure 6.16: Pure elastic deformation in one element test

6.2.1 One-Element Test with HYPEP Model

A one-element test was carried out to verify the hyperelastic plastic ($HYPEP$) material model that we introduced above. A 9-Node element was chosen in this test and the set-up can be seen in Fig. 6.15. The prescribed displacements are given by Node 3, Node 7 and Node 4. Node 1 was suppressed and Node 5 and Node 2 can only move along the X-direction.

There are two ways to test this model. First with only a pure elastic deformation. The element should be spring back 100 percent after unloading. Since the elastic response is derived from a hyperelastic potential, the work done in a closed elastic deformation path vanishes exactly. In Fig. 6.16 one mesh is the deformed mesh with an elastic deformation and the other mesh is the mesh with pure elastic spring-back. It was found that the mesh had

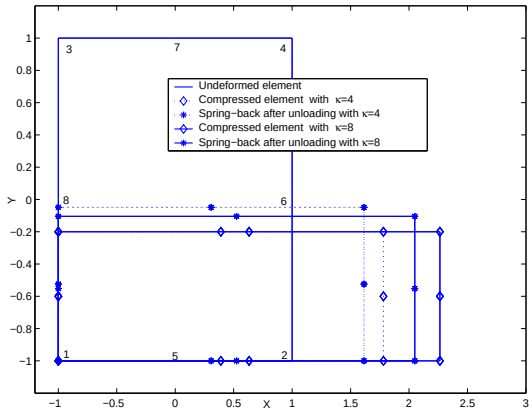

Figure 6.17: Two elastic plastic deformations in one-element test

sprung back to the undeformed state. Secondly an elasto-plastic deformation was carried out in the procedure above. After a certain amount of reduction the element was unloaded with two different elasto-plastic deformations. In these two deformations the material parameter κ was changed. It can found in Fig. 6.17. From this one-element test, this hyperelastic plastic material model can be applied for further research.

6.2.2 Simple Extrusion Test with HYPEP Model

This extrusion test has the same upsetting and calculation as the example in Section 6.1.2, but the material model is changed to a hyperelastic plastic material model ($HYPEP$). Another difference is that a larger reduction has been applied in this case. The material proprieties was chosen as follows in Table 6.3. The friction coefficient was chosen to be 0.1.

The deformed mesh with the velocity plot is shown in Fig. 6.18. The

κ	μ	E_t	S_{y0}	$[v_X, v_Y](m/s)$
160Gpa	80Gpa	2Gpa	1Gpa	[1 0]

Table 6.3: The material parameters of extrusion case in nonlinear model

deformed mesh with equivalent strains distribution is shown in Fig. 6.19. The values in the largest loading region were larger than those in the flow-out area due to the elastic spring-back. The deformed mesh with equivalent plastic strains is shown in Fig. 6.20. It is seen that the equivalent plastic strains reach constant values from the deformed area.

The material properties play an important role in the deformation. In Fig. 6.21 two deformed meshes have a different deformation when these

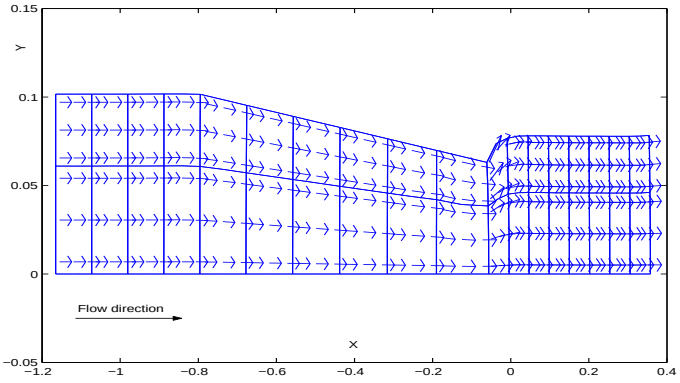

Figure 6.18: Deformed mesh with velocity vector plot

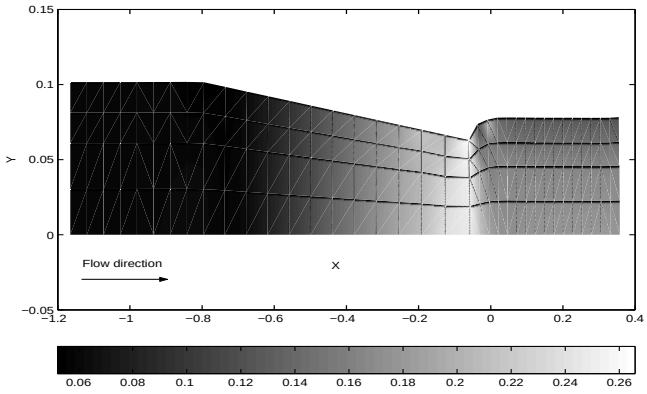

Figure 6.19: Equivalent total strain distribution

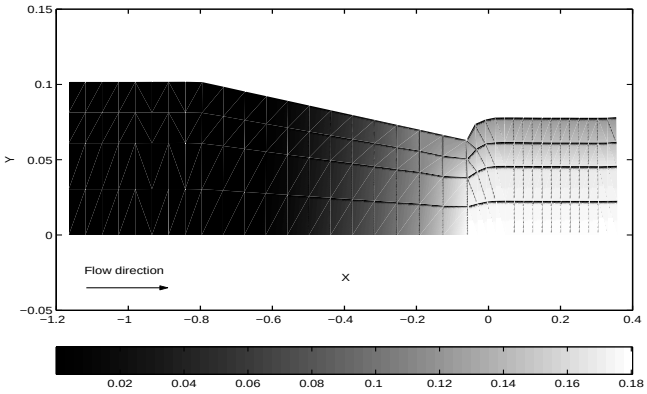

Figure 6.20: Equivalent plastic strain distribution

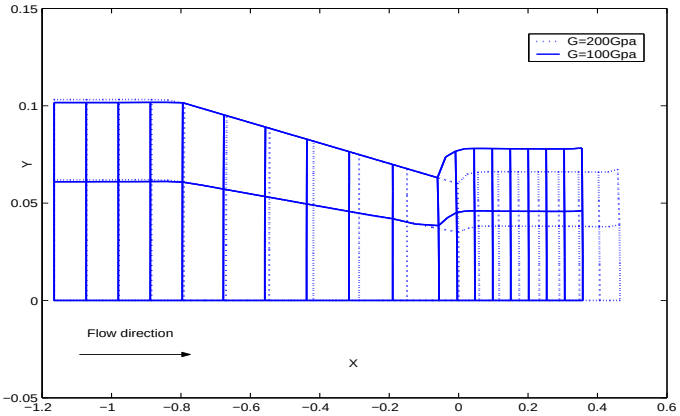

Figure 6.21: Equivalent total strains distribution

deformations were carried out with different bulk moduli.

6.3 Conclusions

In this chapter the developed steady state formulation was applied for different material models, which can be used for small or large deformation cases. As shown in these samples the elastic spring-back can be obtained directly after flowing out.

Bibliography

[1] Belytschko, T., Liu, W.K., Moran, B.: Nonlinear finite elements for continua and structures. John Wiley and Sons Ltd., England, 2001

[2] Simo, J.C.: A framework for finite strain elastoplasticity based on maximum plastic dissipation and the mutliplicative decomposition: part I Continuum Formulation, Computer Methods in Applied Mechanics and Engineering. Vol. 66, 199-219, 1988

[3] Simo, J.C.: A framework for finite strain elastoplasticity based on maximum plastic dissipation and the mulitplicative decomposition: part II Computational Aspects,Computer Methods in Applied Mechanics and Engineering. Vol. 68, 1-31, 1988

[4] Simo, J.C., Hughes, T.J.R.: Computational inelasticity, spring-Verlag, New York, Inc., 241-261 301-307, 1988

[5] Bonet, J., Wood, R.D.: Nonlinear continuum mechanics for finite element analysis, Cambridge University Press, 1997

[6] Balagangadhar, D., Tortorelli,D.A.: Design of large-deformation steady elastoplastic manufacturing processes. Part I: A displacement-based reference frame formulation. International Journal for Numerical Methods in Engineering. Vol. 49, 2000, 899-932

[10] Balagangadhar, D., Dorai, G.A., Tortorelli, D.A.: A displacement-based reference frame formulation for steady-state thermo-elasto-plastic material processes. International Journal of Solids Structures. Vol. 36, 1999, 2397-2416

[8] Belytschko, T., Liu, W.K., Moran, B.: Nonlinear finite elements for continua and structures. John Wiley and Sons Ltd., England, 2001

[10] Yu, Y., Geijselaers, H.J.M., Huétink, J.: A new displacement based FE formulation for steady state problems, Simulation of Materials Processing: Theory, Methods and Applications,Mori (Eds), Proceedings of NUMIFORM 2001, Toyohashi, Japan, 2001, 121-126

[10] Yu, Y.: A new displacement based FE formulation for steady state problems, Intern report of N.I.M.R (P.00.4.021), 2000

Chapter 7

Conclusions and Recommendations

An end and also a beginning

7.1 Conclusions

The aim of the research was to develop a new displacement based formulation for steady state flow processes and to test this formulation using the finite element method. In our study the material evolution equation of any state variable for steady state is derived as:

$$\dot{f} = \boldsymbol{v}_0 \cdot \nabla_{\mathbf{0}} f \tag{7.1}$$

This is a key equation for the development of our new displacement based formulation for the steady state problems. Even though in Balagangdhar's work (See Chapter 3) the material evolution is also related to the known velocity field, the material evolution equation must be transformed to that reference configuration. This kind of performance makes the procedure complicated and not easy to understand. However, in our displacement based formulation, two basic equations (the equilibrium equation and the material evolution equation) can be expressed in the undeformed configuration and hence be solved more simply than in the work of Balagangdhar. In our case the equations to be solved are uncoupled.

The developed formulation differs from the three common descriptions: Lagrangian, Eulerian and ALE descriptions, which have been used widely to model steady state flow processes in recent years. Compared to these descriptions our method has the following advantages and differences:

1. A transient analysis is not required as the reference fields do not vary with time in the steady state situation. The displacements and plastic strains are the primary variables.

2. Elastic spring-back can be obtained directly because the plastic parameter can be calculated from its rate form.

3. The material evolution equations in the reference configuration have a similar expressions as those in the Eulerian configuration. Integration of these equations does not require time integration, since these equations are dependent only on the inflow velocity and the undeformed contact region. Therefore the integration of the material evolution equations was carried out along the known streamlines. The free surface corrections are unnecessary.

4. Contact problems cannot be treated as in the conventional way in the Lagrangian, Eulerian and ALE formulations (Chpater 5).

In fact, this new method combines features of the Lagarangian and Eulerian formualtions.

During the solution of this formulation using FEM, the following should be taken into account:

1 One problem is how to obtain the time derivatives of the state variables. When using the second gradient of the displacement ([1]) to directly obtain the time derivatives of the state variables, a disagreement with the exact solutions in the elastic deformation was found in our study (See Section 5.2.3), especially for the shear stresses. Therefore, an improvement was made, in which the time derivatives of the state variables were calculated form the average nodal strains. The results were much better than using the second gradient of the displacement, even though there were still local deviations.

2. Mostly the streamline upwind Petrov-Galerkin (SUPG) method has been applied to solve the convection equations in the literature. However, in our work the Least Squares (LS) method was applied to solve the material state evoultion equations because this method gives more stable solutions than the SUPG method, as shown in Section 5.2.2.

3. A contact algorithm was developed in which the contact force is treated as the external force, in our case in global equilibrium equation. This contact method is different from the contact methods in transient calculations or impact problems.

Overall, it should be mentioned that this research field is still new and more detailed work must still to be carried out because the current research is restricted to simple geometry, elastoplasticity, and a rigid tool contact. However, this formulation provides the researcher and the engineer with a new strategy in simulation of steady state flow processes.

7.2 Recommendations

As mentioned above, our current research presented some limits and problems as follows:

1. In our work, a simple tool geometry was applied. In order to apply this steady state formulation in real industrial process modelling, a more complicated tool should be included in further research.

2. The elastic plastic material model was used in our work, however, as we know visco-elastoplastic material models are used widely in metal forming process simulation. It is important that this kind of model is implemented in the developed steady state formulation.

3. How to apply a $3D$ analysis to this formulation is also of great interest.

4. The contact problem is always a big issue which should not be ignored. In our work the tool is assumed rigid and smooth, and hence the contact algorithm must be improved for the non-rigid problem.

5. Other steady manufacturing processes should be tested using this formulation.

Bibliography

[1] Balagangadhar, D.: A reference frame formulation for the analysis and design of steady manufacturing processes, PhD thesis, UIUC, USA, 1999

[2] Yu, Y., Geijselaers, H.J.M., Huétink, J. : A new displacement based FE formulation for steady state problems, Simulation of Materials Processing: Theory, Methods and Applications, Mori (Eds), Proceedings of NUMIFORM 2001, Toyohashi, Japan, 2001, 121-126

Appendix A

Proof of Equation (3.45)

$\mathbf{X}$ and $\mathbf{r}$ represent two Cartesian coordinate systems, with related to:

$$\mathbf{X} = \mathbf{R}(t)\mathbf{r} + \mathbf{X}_T(t) \tag{A.1}$$

in which $\mathbf{r}$ is the rotation tensor and $\mathbf{X}_T$ is the transition vector. In contrast,

$$\mathbf{r} = \mathbf{R}^{-1}(t)(\mathbf{X} - \mathbf{X}_T(t)) \tag{A.2}$$

Therefore:

$$\begin{aligned}
&\frac{\partial \mathbf{r}}{\partial t}|_{\mathbf{X}} + \frac{\partial \mathbf{r}}{\partial \mathbf{X}}\frac{\partial \mathbf{X}}{\partial t}|_{\mathbf{r}} \\
&= \mathbf{R}^{-1}(\dot{\mathbf{R}}\mathbf{r} + \dot{\mathbf{X}}_T) + (\dot{\mathbf{R}}^{-1}\mathbf{X} - \dot{\mathbf{R}}^{-1}\mathbf{X}_T - \dot{R}^{-1}\dot{\mathbf{X}}_T) \\
&= \mathbf{R}^{-1}\dot{\mathbf{R}}\mathbf{r} + \dot{\mathbf{R}}^{-1}\mathbf{X} - \dot{R}^{-1}\mathbf{X}_T \\
&= \mathbf{R}^{-1}\dot{\mathbf{R}}\mathbf{r} + \dot{\mathbf{R}}^{-1}(\mathbf{R}\mathbf{r} + \mathbf{X}_T) - \dot{R}^{-1}\mathbf{X}_T \\
&= \mathbf{R}^{-1}\dot{\mathbf{R}}\mathbf{r} + \dot{\mathbf{R}}^{-1}\mathbf{R}\mathbf{r} \\
&= (\mathbf{R}^{-1}\mathbf{R})^{\cdot}\mathbf{r} \\
&= 0
\end{aligned} \tag{A.3}$$

Appendix B

Voigt Notation

In finite element implementations, symmetric second-order tensors (e.g. for the stresses and the strains) are written as column matrices in order to simplify the tensor calculations. Any other conversion procedure of higher-order tensors to matrices is called the Voigt notation.

For example, the material tangent moduli tensor $\mathbf{C}^{\mathbf{S}}_{ijkl}$ is a fourth order tensor and it complicates the programming procedure. In index notation the linear elastic law is written as:

$$\mathbf{S}_{ij} = \mathbf{C}^{S}_{ijkl}\mathbf{E}_{kl} \tag{B.1}$$

The Voigt matrix form of the above is:

$$\mathbf{S}_{a} = \mathbf{C}^{S}_{ab}\mathbf{E}_{b} \tag{B.2}$$

where $a \leftarrow ij$ and $b \rightarrow kl$ as in Table A2.1 in plane strain case.

$\mathbf{C}^S_{ijkl}$		$\mathbf{C}^S_{ab}$	
ij	kl	a	b
11	11	1	1
11	22	1	2
11	33	1	3
11	12	1	4
22	11	2	1
22	22	2	2
22	33	2	3
22	12	2	4
33	11	3	1
33	22	3	2
33	33	3	3
33	12	3	4
12	11	4	1
12	22	4	2
12	33	4	3
12	12	4	4

Table A2.1 voigt rule for plane strain

Appendix C

dN, $\nabla_{\mathbf{u}} dN, \nabla_{\mathbf{u}} \nabla_{\mathbf{u}} dN$

See the figure below,

$$dN = \frac{\mathbf{n}}{\|\mathbf{n}\|}^T \cdot \mathbf{b}_1\mathbf{a} \tag{C.1}$$

$$\mathbf{n} = \mathbf{M} \cdot \mathbf{b}_1\mathbf{b}_2 \tag{C.2}$$

M is a rotating matrix to obtain the normal vector. $\mathbf{b}_1\mathbf{a}$ represents a vector from point b_1 to point a:

$$\mathbf{b}_1\mathbf{a} = \underline{\mathbf{a}} - \underline{\mathbf{b}_1} \tag{C.3}$$

Therefore:

$$\nabla_{\mathbf{u}} dN = \frac{\mathbf{n}}{\|\mathbf{n}\|}^T \cdot \nabla_{\mathbf{u}} \mathbf{a}\mathbf{b}_1 + \mathbf{a}\mathbf{b}_1{}^T \cdot \nabla_{\mathbf{u}} \frac{\mathbf{n}}{\|\mathbf{n}\|} \tag{C.4}$$

since $\mathbf{a}$ is a linear function of $\mathbf{u}$:

$$\nabla\nabla_{\mathbf{u}} dN^T \approx \nabla_{\mathbf{u}} \frac{\mathbf{n}}{\|\mathbf{n}\|}^T \cdot \nabla_{\mathbf{u}} \mathbf{a}\mathbf{b}_1 + \nabla_{\mathbf{u}} \mathbf{a}\mathbf{b}_1{}^T \cdot \nabla_{\mathbf{u}} \frac{\mathbf{n}}{\|\mathbf{n}\|} \tag{C.5}$$

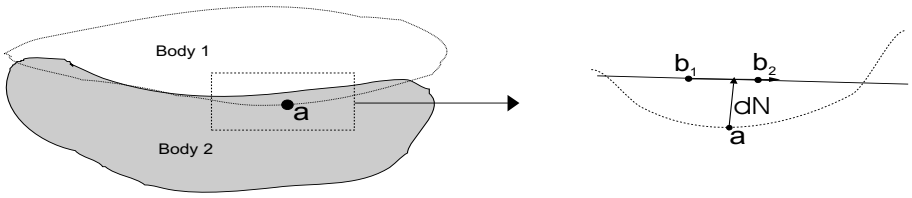

Figure C.1: Digram illustrating the gap definition between two contacting bodies

Appendix D

dt, $\nabla_{\mathbf{u}} dt$ for Impact Problem

The contact slave node **a** of body 1 moves from calculation step i to calculation step $i+1$. At every step the projection of **a** on body 2 can be calculated. The slip of this slave node will be zero within one step and only occurs between two calculation steps. Therefore the slip distance can be treated as the distance between the projections of **a** on body 2 during two steps. Body 2 is divided into elements in the finite element method. Therefore, the gradient of dt and the second order difference of dt can be obtained through several tensor calculations as follows(see Fig. D.1): Step i:

$$\bar{\alpha} = \frac{1}{\|\bar{\mathbf{b}}_k \bar{\mathbf{b}}_{k+1}\|} \bar{\mathbf{b}}_k \bar{\mathbf{a}} \cdot \bar{\mathbf{b}}_k \bar{\mathbf{b}}_{k+1} \qquad \bar{\alpha} \in [0,1] \tag{D.1}$$

The overbar denotes the quantities related to the configuration of step i.
Step $i+1$:

Body 2 changes its position related to reference configuration (due to stretch or shrink), and this kind of change should be considered while the slip is calculated.

The projection of a in step i on Body 2 will also change due to stretching

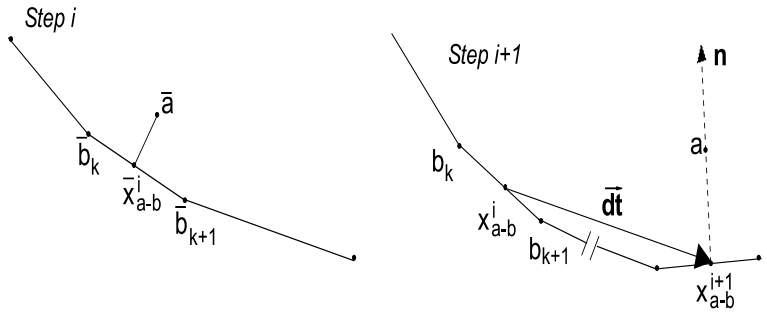

Figure D.1: Schematic depicting slip vector between two bodies

or shrinking of body 2 in step $i+1$, but the relative position of the projection in $\mathbf{b}_k\mathbf{b}_{k+1}$ will be the same as in step i, therefore:

$$\frac{\|\mathbf{b}_k\bar{\mathbf{a}} \cdot \mathbf{b}_k\mathbf{b}_{k+1}\|}{\mathbf{b}_k\mathbf{b}_{k+1}} = \bar{\alpha} \tag{D.2}$$

The coordinate of the projection of $\mathbf{a}$ on body 2 in step i ($\mathbf{x}^i_{a-b}$) related to the configuration in step $i+1$ can be calculated as:

$$\mathbf{x}^i_{a-b} = (1-\bar{\alpha})\mathbf{x}_{b_k} + \bar{\alpha}\mathbf{x}_{b_{k+1}} \tag{D.3}$$

Further on, in step $i+1$, $\mathbf{a}$ moves to the new situation due to deformation from step i to step $i+1$, the coordinate of projection $\mathbf{a}$ in step $i+1$ can be expressed as:

$$\mathbf{x}^{i+1}_{a-b} = \mathbf{x}_a - dN^{i+1} \cdot \frac{\mathbf{n}^{i+1}}{\|\mathbf{n}^{i+1}\|} \tag{D.4}$$

The slip vector can be obtained:

$$\mathbf{dt} = \mathbf{x}^{i+1}_{a-b} - \mathbf{x}^i_{a-b} = \mathbf{x}_a - \mathbf{dN} \cdot \frac{\mathbf{n}}{\|\mathbf{n}\|} - (1-\bar{\alpha})\mathbf{x}_{b_1} - \bar{\alpha}\mathbf{x}_{b_2} \tag{D.5}$$

The size of $\mathbf{dt}$ is:

$$dt = \|\mathbf{dt}\| = \sqrt{\mathbf{dt}^T \cdot \mathbf{dt}} \tag{D.6}$$

The gradient of dt is:

$$\nabla_{\mathbf{u}} dt = \frac{\mathbf{dt}^T \cdot \nabla_{\mathbf{u}}\mathbf{dt}}{dt} \tag{D.7}$$

with:

$$\nabla_{\mathbf{u}}\mathbf{dt} = \nabla_{\mathbf{u}}\mathbf{x}_a - \nabla_{\mathbf{u}}(dN \cdot \frac{\mathbf{n}}{\|\mathbf{n}\|}) - (1-\bar{\alpha})\nabla_{\mathbf{u}}\mathbf{x}_{b_1} - \bar{\alpha}\nabla_{\mathbf{u}}\mathbf{x}_{b_2} \tag{D.8}$$

$$\nabla_{\mathbf{u}}(dN \cdot \frac{\mathbf{n}}{\|\mathbf{n}\|}) = dN \cdot \nabla_{\mathbf{u}}\frac{\mathbf{n}}{\|\mathbf{n}\|} + \frac{\mathbf{n}}{\|\mathbf{n}\|} \otimes \nabla_{\mathbf{u}}\mathbf{dN} \tag{D.9}$$

Furthermore, the second derivative of the slip distance should be known for the stiffness matrix:

$$\nabla(\nabla_{\mathbf{u}} dt) = \frac{\mathbf{dt}}{dt}^T \cdot \nabla(\nabla_{\mathbf{u}}\mathbf{dt}) + (\nabla_{\mathbf{u}}\mathbf{dt})^T \cdot (\nabla_{\mathbf{u}}\frac{\mathbf{dt}}{dt}) \tag{D.10}$$

The first term can be treated as zero due to the linearity of the slip vector. Therefore:

$$\nabla(\nabla_{\mathbf{u}} dt) = (\nabla_{\mathbf{u}}\mathbf{dt})^T \cdot (\frac{\nabla_{\mathbf{u}}\mathbf{dt}}{dt} + \mathbf{dt} \otimes \nabla_{\mathbf{u}}\frac{1}{dt}) \tag{D.11}$$

List of Symbols

Scalars

E	Modulus of elasticity
G	Shear modulus
t	Time
f	An arbitrary history-dependent field variable
ϕ	Yield function
J	Jocobian
K	Bulk modulus
$\dot{\gamma}$	Plastic parameter
Ω	Volume
Ω_0	Initial volume
Γ	Surface
Γ_0	Initial surface
V	Volume
ρ	Density
dN	Normal distance between two bodies
W	Power
λ	Lam constant
μ	Lam constant, friction cofficient
$\hat{\psi}$	Stored-energy function
ν	Poisson's ratio
κ	Bulk modulus

Tensors

Vectors

$\mathbf{b}$	Body force
$\mathbf{q}$	Internal variables

$\mathbf{t}$	Traction
$\mathbf{t}_c$	Contact force
$\mathbf{u}$	Displacement
$\mathbf{n}$	Normal vector
$\mathbf{v}$	Velocity
$\mathbf{x}$	A material point in the current configuration
$\mathbf{X}$	A material point in the reference configuration

2nd order tensors

$\mathbf{e}$	Eulerian or Almansi strain tensor
$\mathbf{C}$	Cauchy-Green strain tensor
$\mathbf{D}$	Rate of deformation
$\mathbf{E}$	Green (Green-Lagrange) strain tensor
$\mathbf{F}$	Deformation tensor
$\mathbf{I}$	Unit tensor
$\mathbf{L}$	Velocity tensor
$\mathbf{P}$	First Piola-Kirchhoff stress tensor
$\mathbf{Q}$	Rotation tensor
$\mathbf{S}$	Second Piola-Kirchhoff stress tensor
$\mathbf{W}$	Spin tensor
$\boldsymbol{\tau}$	Kirchhoff stress tensor
$\boldsymbol{\varepsilon}$	Linear strain tensor
$\boldsymbol{\sigma}$	Cauchy stress tensor

4th order tensor

$\mathbf{C}_{el}$	Linear elasticity tensor
$\mathbf{Y}$	Yield tensor

Operators

$\boldsymbol{\phi}$	Mapping operator of points from the material domain to the spatial domain
$\bar{\boldsymbol{\phi}}$	Mapping function of points from the reference domain to the spatial domain

$\mathbf{\Phi}$	Mapping function of points from the material domain to the reference domain
∇	Gradient with respect to current coordinates
∇_0	Gradient with respect to reference coordinates
$\nabla_{\mathbf{u}}$	Gradient with respect to displacements $\mathbf{u}$
$\dot{\beta}$	Material time derivative of β
β^{-1}	Inverse of β
β^T	Transpose of β
$\cdot$	Tensor contraction
:	Double tensor contraction
$\|\beta\|$	Two-norm of β

Sub- and superscripts

i, j	Index
c	Contact issue
e	Elastic
i	Body i
n	Normal
t	Tangential
0	Initial
$\mathbf{x}$	Concerning the deformed configuration
$\mathbf{X}$	Concerning the undeformed configuration

Others

V_0	Undeformed domain
V_m	Referential domain
V	Deformed domain
$tr(\mathbf{A})$	Trace of matrix $\mathbf{A}$
$\mathbf{K}$	Stiffness matrix

Acknowledgements

This project is funded by the Netherlands Institute for Metals Research (NIMR), and takes place within the group of Technical Mechanics of the University of Twente. Their assistance is greatly acknowledged and appreciated.

Many persons have contributed to this thesis:

First I would like to express my sincere appreciation to Han Huétink for offering me the opportunity to do this research. He helped me to better understand the theory of Continuum Mechanics and provided many valuable suggestions and comments to this research.

This thesis could not have been written without Bert Geijselaers who not only served as my supervisor but also encouraged and challenged me throughout this project. He provided me with his insight, recommendations to this research and guidance on writing this thesis. I thank him.

I am grateful to all my colleagues for making my stay at the university of Twente a memorable and valuable experience. Getjan Kloosterman gave significant help on the contact algorithm in this thesis. In addition to that we exchanged lots of views about the world and life in general. The computer assistance and support of Herman Corbach and Nico van Vliet are gratefully acknowledged. I am indebted for the administrative support from Annnemarie Teunissen, Debbie Vrieze, Jacqueline Emmerich and Tanja Gerritsen. Especially to Tanja who helped greatly on my documentation work after I moved to Eindhoven two years ago. Also my thanks to Harm Wisselink, who dedicated time reading part of my thesis and offered comments for improvements, to Ton van den Boogaard, who provided me with the layout template of LATEX and to Katrina Emmett, who checked the English language of this manuscript.

On the home front, I would like to give thanks to my friends in Delft, Enschede and Eindhoven for having made my life more enjoyable. The most pleasant times were playing cards in the weekends, even during my pregnancy.

Last but not least, I would like to dedicate this thesis to my family for their never-ending support. My two sisters who have always supported me

from my childhood. Without the encouragements and love from my parents, this thesis would not have been completed. Papa, I know you are happy to see this come true. Now my words go to my husband Liujin Tang. Thanks for your love, understanding and the happy time you made for me in my life. You always encouraged and supported me to finish this thesis. My lovely little son, Charlie, I admire what you have done and achieved in the last two years (better than your mom). Your pure smile had always refreshed me while writing this thesis.

Yuhong Yu
Eindhoven, November 2004